



Contents lists available at ScienceDirect

## Arabian Journal of Chemistry

journal homepage: [www.ksu.edu.sa](http://www.ksu.edu.sa)

Original article

# Synthesis, evaluation, and computational chemistry of novel selenenyl sulfides as 3C protease inhibitors with strong cell-based antiviral activity

Jin-Yin Tang<sup>a,1</sup>, Shengwang Dai<sup>b,1</sup>, Xiaofang Wang<sup>c,1</sup>, Mengting Zhang<sup>b</sup>, Jin-Rui Shi<sup>a</sup>,  
Yong-Xuan Hong<sup>a</sup>, Zhi-Juan Sun<sup>c</sup>, Huan-Qin Dai<sup>b,d,\*</sup>, Jian-Guo Wang<sup>a,\*</sup>

<sup>a</sup> State-Key Laboratory and Research Institute of Elemento-Organic Chemistry, Frontiers Science Center for New Organic Matter, National Engineering Research Center of Pesticide, College of Chemistry, Nankai University, Tianjin 300071, China

<sup>b</sup> State Key Laboratory of Mycology, Institute of Microbiology, Chinese Academy of Sciences, Beijing 100101, China

<sup>c</sup> Newish Biological R&D Center, Beijing 100176, China

<sup>d</sup> Savaid Medical School, University of Chinese Academy of Sciences, Beijing, 100049, China

## ARTICLE INFO

## Keywords:

3C protease  
Selenenyl sulfides  
Antiviral activity  
Selectivity index  
Computational chemistry

## ABSTRACT

The 3C protease (3C<sup>PRO</sup>) is an important enzyme for developing therapeutic medicines against some severe viral infections. In order to discover new classes of antiviral agents, 42 novel selenenyl sulfides were prepared and characterized by <sup>1</sup>H NMR, <sup>13</sup>C NMR, <sup>77</sup>Se NMR and HRMS. The target compounds demonstrated promising inhibitions against 3C<sup>PRO</sup> from either enterovirus 71 (EV71) or coxsackievirus B3 (CVB3), as well as desirable cell-based antiviral activity against these viruses. Among them, **11f** displayed the most potent IC<sub>50</sub> value of 0.28 ± 0.05 μM against EV71-3C<sup>PRO</sup>, and the strongest IC<sub>50</sub> value of 0.72 ± 0.15 μM against CVB3, with a selectivity index of 51.5 against Hela cell, superior to the control drug rupintrivir. In addition, molecular docking was undertaken to predict a possible binding mode for compound **11f**, and a comparative molecular field analysis (CoMFA) model was subsequently generated to understand the structure-activity relationships. Overall, the present research has provided some new insights to design a distinct family of antiviral compounds.

## 1. Introduction

Diseases caused by some viral infections have been threatening the health of human being seriously, such as severe acute respiratory syndrome (SARS), coronavirus disease 2019 (COVID-19), and enterovirus infections (Krilov, 2004; Li et al., 2021; Nayak et al., 2022). Enterovirus 71 (EV71) is the major pathogen responsible for hand, foot, and mouth disease (HFMD) (Salerno et al., 2023), while CVB3 is associated with aseptic meningitis, hepatitis, meningoencephalitis and chronic dilated cardiomyopathy (Zhu et al., 2023). Although the scales of EV71 and CVB3 outbreaks are not to the level of the COVID-19 pandemic, special attention should be also paid to them in that the existence of these viruses is long-standing and such infections are fatal to some patients. Even if different vaccines have been developed to prevent the prevalence of EV71 or CVB3 related infectious diseases, identification of novel chemical agents is still of vital importance since individuals are often unluckily infected by these picornaviruses.

Among the biological targets involved in the biological reactions of

the picornavirus replication, a highly structurally conserved cysteine protease, namely 3C protease (3C<sup>PRO</sup>), does not exist in human bodies, and this feature has made it an popular target to design novel antiviral compounds (Ramajayam et al., 2011; Stubbing et al., 2023; Zeng et al., 2020). Some efforts were also made to develop covalent inhibitory antibody against human rhinovirus 14 (HRV14) 3C protease through unnatural amino acid mutagenesis in a recent study (Cheng et al., 2021). A similar enzyme from coronaviruses or calciviruses, such as SARS-CoV or SARS-CoV-2, is called 3C-like protease (3CL<sup>PRO</sup>). Continuous efforts have been devoted to identifying new agents that inhibit the proteases, especially in the battle against the COVID-19 pandemic (Han et al., 2022; Luz et al., 2023; Mohammad et al., 2020; Tan et al., 2023; Wang et al., 2022; Yoosefian et al., 2023; Zhang et al., 2020). Traditional inhibitors that target 3C<sup>PRO</sup> or 3CL<sup>PRO</sup> include peptidomimetic compounds and natural products, such as rupintrivir (AG7088), nirmatrelvir (PF-07321332), baicalein, and DC07090 (Cannalire et al., 2022; Chen et al., 2023; Zang et al., 2022).

Some synthesized aromatic disulfides were identified as novel

\* Corresponding authors at: State Key Laboratory of Mycology, Institute of Microbiology, Chinese Academy of Sciences, Beijing 100101, China (H.Q. Dai).

E-mail addresses: [daihq@im.ac.cn](mailto:daihq@im.ac.cn) (H.-Q. Dai), [nkwjg@nankai.edu.cn](mailto:nkwjg@nankai.edu.cn) (J.-G. Wang).

<sup>1</sup> J.-Y. Tang, S. Dai and X. Wang contributed equally to this work.

<https://doi.org/10.1016/j.arabjc.2024.105713>

Received 6 December 2023; Accepted 5 March 2024

Available online 11 March 2024

1878-5352/© 2024 The Author(s). Published by Elsevier B.V. on behalf of King Saud University. This is an open access article under the CC BY-NC-ND license (<http://creativecommons.org/licenses/by-nc-nd/4.0/>).

inhibitors (Example 1) of SARS-CoV-3CL<sup>pro</sup> but no covalent bond was observed to form with the enzyme (Wang et al., 2017). A clinical drug disulfiram was reported to exhibit some antiviral activity against COVID-19 (Jin et al., 2020). Selenium is an essential micronutrient for human health and insufficient intake of this element from daily diet will result in many disease (Sanmartin et al., 2011). For this reason, organoselenium compounds have attracted much attention and these compounds displayed versatile biological activities (Chipoline et al., 2022; Singh and Kunwar, 2021). As a representative selenium-containing organic compound, ebselen has been famous for its anti-inflammatory, antibacterial, and antioxidant activities (Maślanka and Mucha, 2023; Noguchi, 2016; Parnham and Sies, 2000). In the early stage of the COVID-19 outbreak, ebselen was identified as a potent inhibitor of SARS-CoV-2-3CL<sup>pro</sup> and it showed promising antiviral activity against SARS-CoV-2 in cell-based assay (Jin et al., 2020). Previously, some selenenyl sulfide compounds were synthesized and a few of them (Example 2) exhibited desirable activities against tobacco mosaic virus (TMV), showing a great potential for the development of new agrochemicals (Shang et al., 2023). Fig. 1 illustrates the chemical structures of all the examples mentioned above.

Given the advances in the biological activities of disulfides or selenenyl sulfide compounds that have been mentioned above and the fact that very limited drugs are clinically available for the treatment of EV71 or CVB3 infections and, it is worth exploring novel compounds containing selenenyl sulfide frameworks to identify different agents to combat these risky diseases. Bearing these in mind, synthesis of new selenenyl sulfides and evaluation of their biological activities against 3C<sup>pro</sup>, together with the cell-based antiviral activity, is expected to be a preferable solution to offer some new chemical family of inhibitors that are effective upon EV71 or CVB3. This idea has been realized in this paper and **11f** was identified as a stronger inhibitor than the control drug rupintrivir, as well as improved selectivity index. Since it is very challenging for the innovation of drugs that target 3C<sup>pro</sup>, the current research will provide some insight for lead discovery against these viral infectious diseases for further consideration.

## 2. Results and discussion

### 2.1. Chemistry of the compounds

Aiming at investigating the influence of aliphatic groups (R<sup>1</sup>) and aromatic groups (R<sup>3</sup>) in the compounds, two different series, **7a-7u** and **11a-11u** were synthesized. The chemical routes are shown in Scheme 1 and Scheme 2, respectively. Although both compounds **7a-7u** and **11a-11u** were prepared via nucleophilic substitutions, corresponding reactions for these two series were different. Generally, **7a-7u** were synthesized using a similar method to our previous work (shang et al., 2023), and a modification was that all intermediates **5** were synthesized from **4** in the presence of selenium powder, nano-Copper(I) iodide, and other related reagents. In comparison, compounds with close structure to **11a-11u** have not been reported and the chemistry for the preparation of these compounds will be discussed. The starting material **8** (methyl 2-aminobenzoate or ethyl 2-aminobenzoate) was made into a diazonium salt **9** at iced temperature, after that potassium selenocyanate was added to the reactant in an acidic solution to give intermediate **10** (methyl 2-selenocyanatobenzoate or ethyl 2-selenocyanatobenzoate) in high yields, based on a known procedure (Diesendruck et al., 2009). Finally, **11a-11u** were prepared by reacting **10** with different aromatic thiols **6** using aluminum oxide as a catalyst in dichloromethane at room temperature. The yields for **7a-7u** were in the range of 7–85 % and those for **11a-11u** were from 14 % to 67 %, respectively. Besides <sup>1</sup>H NMR and <sup>13</sup>C NMR, all the selenenyl sulfides were also characterized by <sup>77</sup>Se NMR that is unique for the organoselenium compounds. The spectra of <sup>1</sup>H NMR, <sup>13</sup>C NMR, <sup>77</sup>Se NMR, and HRMS for all the target compounds could be found in the supplementary data. Interestingly, for compounds from both **7** and **11** series, there existed a trend for the isomer compounds with only *ortho* or *para* position difference when R<sub>2</sub> group was a substituted phenyl ring, that the *ortho* substituted compound had a smaller <sup>77</sup>Se NMR chemical shift than the corresponding *para* substituted compound. Such phenomena could be observed from the following pairs of selenenyl sulfides: **7f** (597.0) versus **7g** (566.7), **7i** (597.8) versus **7m** (573.1), **7o** (594.9) versus **7p** (571.2), **11a** (602.9) versus **11f** (567.1), **11b** (615.7) versus **11g** (594.1), **11c** (597.0) versus **11h** (561.0), **11d** (594.3) versus **11i** (561.8), **11n** (597.3) versus **11r**

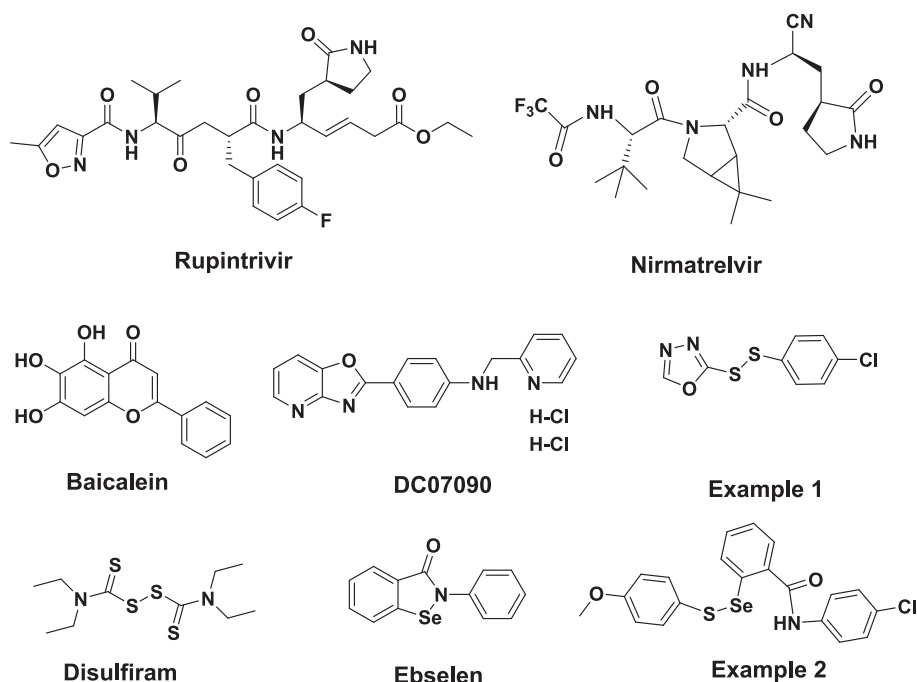
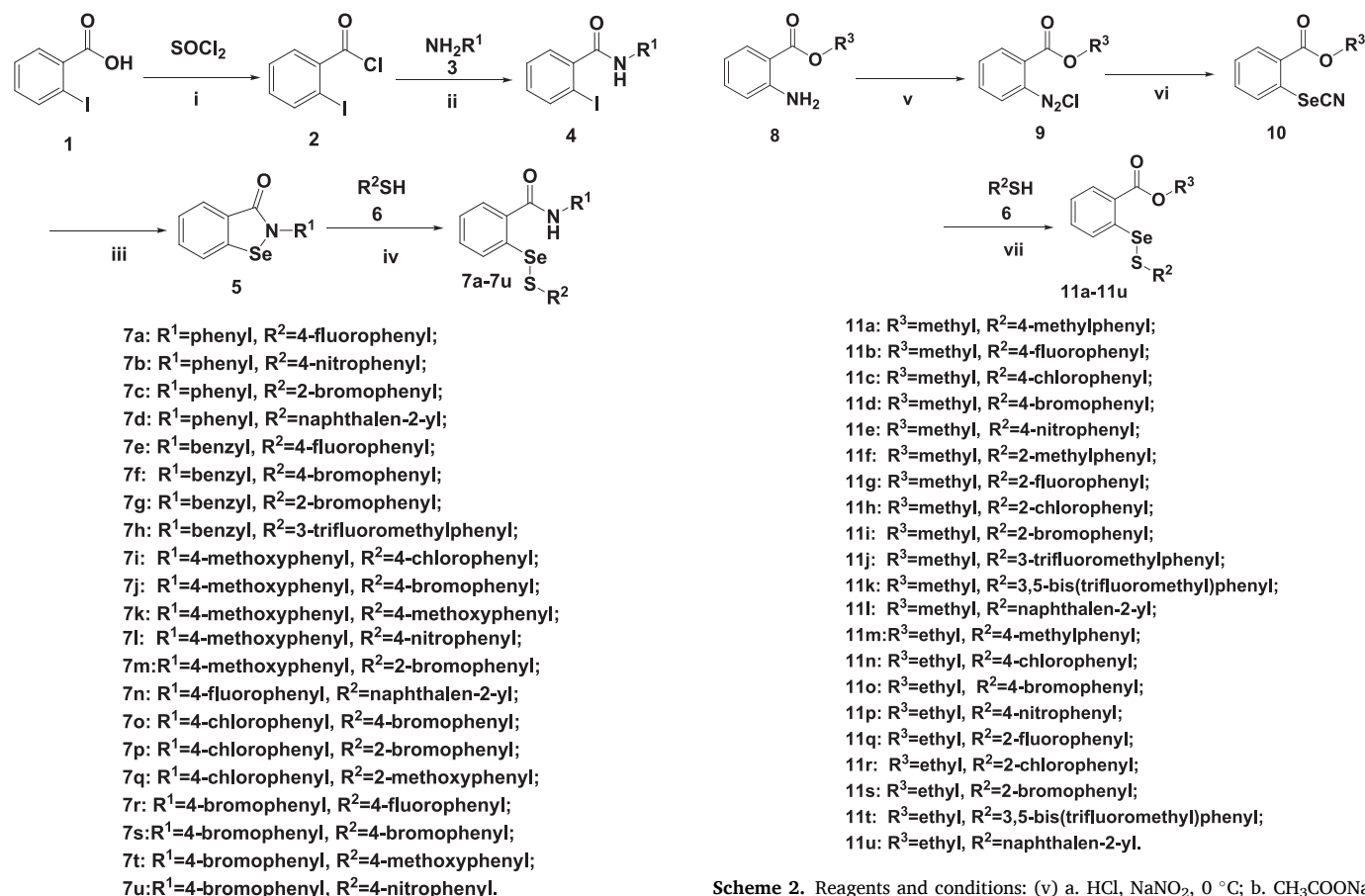


Fig. 1. Molecular structures of Rupintrivir, Nirmatrelvir, Baicalein, DC07090, Examples 1&2, Disulfiram and Ebselen.



**Scheme 1.** Reagents and conditions: (i) Reflux; (ii) Et<sub>3</sub>N, DCM, 0 °C to r.t.; (iii) Se, *t*-BuOK, nano-CuI, 1,10-phenanthroline, DMF, 110 °C; (iv) DCM, r.t.

(558.7), and **11o** (594.2) versus **11s** (562.0), which was in agreement with the results in a previous study (Shang et al., 2023).

In order to confirm the chemical structures in the series of **11a-11u**, single crystals of **11s** (CCDC number 2172212) suitable for X-ray diffraction were successfully obtained using a self-evaporation method in a mixed solution of hexane/dichloromethane (v/v = 100:1), after attempts on a few compounds. From Fig. 2, it can be seen that the molecule adopted an extended conformation in the crystal, from which a Se-S bond was successfully constructed between two phenyl rings and the ester part was linked with the left phenyl ring neighboring to the selenium atom (Se1 in the figure).

Simply from the view of chemistry, although limited compounds in the two series of selenenyl sulfides were synthesized in this study, more compounds with different structures could be considered for investigation. For example, the introduction of iodine atom to the structures might be an interesting topic, as previously shown as halide system (Lun et al., 2023).

## 2.2. Biological activity

The target selenenyl sulfides were all subjected to enzyme inhibitions against EV71-3C<sup>PRO</sup> and CVB3-3C<sup>PRO</sup>, and *in vitro* cell-based evaluations against these two viruses, the results of which have been summarized in Table 1. Generally, most compounds exhibited potent inhibitions against 3C<sup>PRO</sup> and ideal *in vitro* antiviral activities. In order to filter those with very weak inhibitions, the cutoff of IC<sub>50</sub> value was set to 10 μM for 3C<sup>PRO</sup> and that was 30 μM for the cell-based activity. For comparison, rupintrivir was chosen as a control in this study.

Amongst the compounds, **7b**, **7c**, **7d**, **7f**, **7g**, **7i**, **7l**, **7o**, **7p**, **7q**, **7r**,

**Scheme 2.** Reagents and conditions: (v) a. HCl, NaNO<sub>2</sub>, 0 °C; b. CH<sub>3</sub>COONa, 0 °C to r.t.; (vi) KSeCN, H<sub>2</sub>O, r.t.; (vii) Al<sub>2</sub>O<sub>3</sub>, DCM, r.t.

**11a**, **11b**, **11e**, **11f**, **11g**, **11j**, **11m**, **11o**, **11q**, **11t**, and **11u** had IC<sub>50</sub> values < 10 μM for both proteases; **7a**, **7s**, **7t**, and **11k** had IC<sub>50</sub> values < 10 μM for EV71-3C<sup>PRO</sup>; and **7j**, **7k**, **7m**, **11c**, **11d**, **11h**, **11i**, **11n**, **11p**, **11r**, and **11s** had IC<sub>50</sub> values < 10 μM for CVB3-3C<sup>PRO</sup>, respectively. While for **7e**, **7h**, **7n**, **7u** and **11l**, both the IC<sub>50</sub> values against EV71-3C<sup>PRO</sup> and CVB3-3C<sup>PRO</sup> were > 10 μM. For the EV71-3C<sup>PRO</sup> inhibitions, **7b**, **7l**, **7t**, **11g**, **11j**, and **11u** had IC<sub>50</sub> values < 2.5 μM, among which **11f** had the best IC<sub>50</sub> value of 0.28 ± 0.05 μM, much stronger than that of rupintrivir (1.03 ± 0.53 μM). For the CVB3-3C<sup>PRO</sup> inhibitions, **11f**, **11g**, **11h**, and **11u** had IC<sub>50</sub> values < 2.50 μM, comparable to that of rupintrivir (2.01 ± 0.22 μM). Fig. 3a and 3b. display the inhibition curves of **11f** against EV71-3C<sup>PRO</sup> and CVB3-3C<sup>PRO</sup>. Regarding a simple structure-activity relationship, when R<sup>2</sup> was a 4-nitrophenyl group for compound **7**, two of the compounds displayed the best inhibitions against EV71-3C<sup>PRO</sup> (**7b** and **7l**). However, this group did not give strong enzyme inhibitions for **7u**, as well as the corresponding compounds for **11** (**11e** and **11p**). For compound **11**, when R<sup>2</sup> was a 2-methylphenyl group, 2-fluorophenyl group or 3-trifluoromethylphenyl group, potent enzyme inhibitions were observed (**11f**, **11g** and **11j**). However, 3-trifluoromethylphenyl group in **7h** showed very poor enzyme inhibition. When R<sup>2</sup> was a naphthalene-2-yl, **11u** gave strong inhibitions for both 3C<sup>PRO</sup>,

nevertheless, **11l** exhibited no activity even at 10 μM.

It is a concern whether the target selenenyl sulfides inhibit the 3C protease through a covalent bonding manner. From the previous study, the aromatic disulfides did not form a covalent bond with the cysteine residue of SARC-CoV-3CL<sup>PRO</sup> in the active site, which was evidenced by that fact that mass spectrometry of the protease had not been changed and the nonsymmetrical disulfides were reversible inhibitors (Wang et al., 2017). In another study, the selenenyl-cysteine adduct was not found with Cys145 of SARS-CoV-2-3CL<sup>PRO</sup>, using LC-MS/MS analysis of

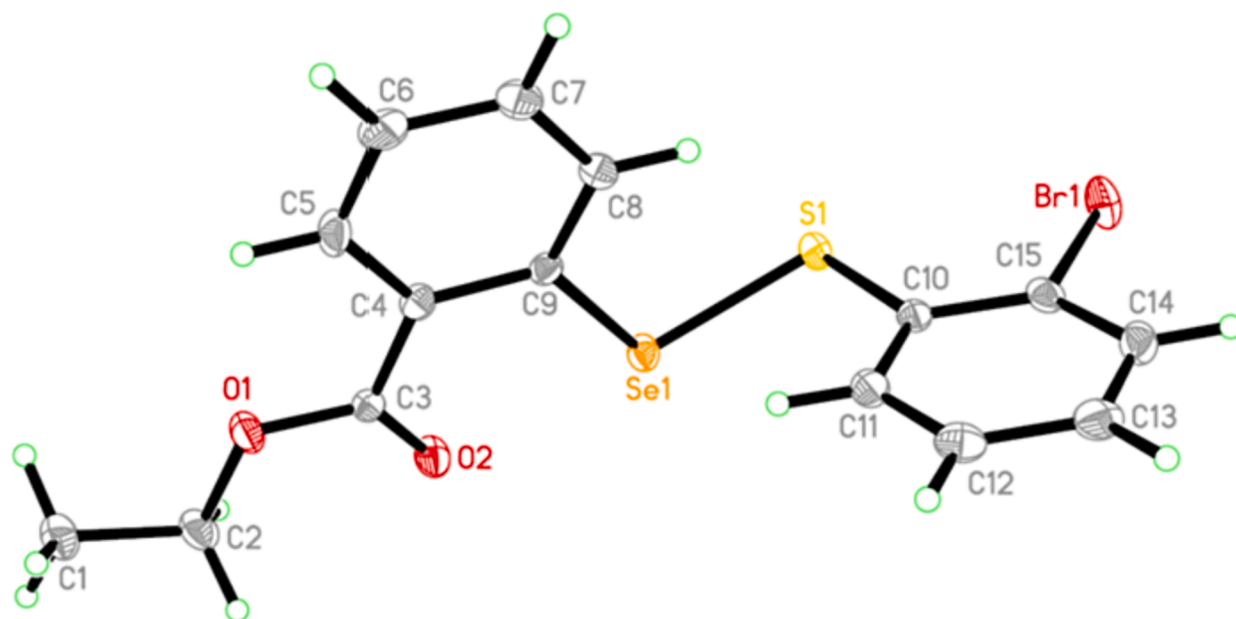


Fig. 2. Crystal structure of compound 11 s.

the tryptic digest of the enzyme, although such an adduct was observed in the ebselen-treated human glutathione S-transferase-pi (Ampornadnani et al., 2021). In this study, inhibition type of the **11f** was further determined by means of enzymatic kinetic behaviors, from which a competitive inhibition behavior was observed and it implied the inhibition was a reversible action (Fig S1). Due to all these reasons, it is quite likely that the selenenyl sulfides do not form covalent bond with the cysteine in the active site of the 3C proteases.

Based on the cell-based evaluation, none of **7 h**, **7i**, **11j**, **11l**, and **11n** had good activities against both EV71 and CVB3, **7a**, **7g**, **11o**, **11p**, **11k**, **11s** and **11t** had one  $IC_{50}$  value  $> 30 \mu M$  against either EV71 or CVB3, and all the other selenenyl sulfides showed  $IC_{50}$  values of  $< 30 \mu M$  against the two viruses. For the cell-based activities against EV71, **11f** and **11u** displayed  $IC_{50}$  values of  $< 2.50 \mu M$ , which were the best ones among all the compounds but still weaker than that of rupintrivir ( $0.74 \pm 0.22 \mu M$ ). For the antiviral activities against CVB3, the  $IC_{50}$  values of **11e** and **11f** were  $1.15 \pm 0.04 \mu M$  and  $0.72 \pm 0.15 \mu M$ , respectively, which were several folds stronger the value of rupintrivir ( $6.52 \pm 0.09 \mu M$ ). Fig. 4a shows the dose–response curve of **11f** against CVB3. Although the cell-based assay is a simple *in vitro* model, it is obvious that the properties of absorption, distribution, metabolism and excretion (ADME) should be taken for consideration for the cellular activity, since the cellular environment is much more complex than the pure enzyme inhibition. Therefore, it was not strange that there did not exist an absolute correlation between the enzyme inhibition and the antiviral activity for the tested selenenyl sulfides. On the other hand, there exists such a possibility, that the antiviral activity of these selenenyl sulfides might involve targeting other viral proteins or host proteins in addition to  $3C^{pro}$ . This is due to a fact that ebselen and some other compounds did not inhibit the viral replication of EV-A71, although those compounds inhibited cysteine proteases significantly (Ma et al., 2020).

The antiviral activity was further supported by viral plaque assay, compound **11f** showed very strong reduction of CVB3 particle formation activity at  $5 \mu M$ , with 80 % inhibition as compared to DMSO controls (Fig. 4b). A subsequent cell cytotoxicity assay for **7q**, **7r**, **7s**, **11e**, **11f**, **11g**, **11u** and rupintrivir against normal Hela cells revealed that selectivity indexes for these compounds were 6.6, 9.4, 8.2, 23.6, 51.5, 6.8, 7.0, and 7.6 for CVB3, respectively (Table 2). Taken together, **11f** was identified as a potent antiviral agent targeting  $3C/3CL^{pro}$  with advantageous bio-safety.

For a general comparison of the antiviral efficacies of between the two series **7a-7u** and **11a-11u**, compounds belonging to the second panel exhibited stronger cell-based antiviral activity. For the anti-CVB3 activity, the  $IC_{50}$  values of **11e** and **11f** were around  $1 \mu M$ , however, none of the compounds from the first series was at the same level. This implied that more attention should be paid to compounds with aliphatic groups ( $R^1$ ) for the next round of molecular design to discover more potent compounds.

Regarding to whether the ester or the amide part of the selenenyl sulfides are stable in the cell-based assay, there is an assumption that the active component in the cellular environment is possible to be the hydrolyzed product. Nevertheless, this might not be true based on the following fact: **7b**, **7l**, **7u**, **11e** and **11p** had same  $R^2$  groups, however, the antiviral activities of them differed significantly. Otherwise, these compounds tended to demonstrate similar antiviral activity. Further experiments will be conducted to study the components after the cell-based assay for a detailed investigation.

In a previous result, we screened a big library of disulfide compounds against CVB3- $3C^{pro}$  and evaluated their cell-based anti-CVB3 activities. Although some compounds showed submicromolar  $IC_{50}$  values against CVB3- $3C^{pro}$ , the antiviral activities were very poor even at  $10 \mu g/mL$  concentration (corresponding to approximately  $30-40 \mu M$  based on different molecular weight of each compound), much weaker than that of rupintrivir at the same condition. That work was not published in a scientific paper, but shown in a patent application (Zhang et al., 2016). The present result suggested that although selenenyl sulfides are bioisosteres of the disulfide compounds, the former have more preferable biological behavior in the cell-based antiviral assay and have much greater potential for further development of novel antiviral agents.

Hundreds of papers have been published on the discovery of inhibitors of SARS-CoV-2 since the outbreak of COVID-19, however, there were very few reports on the identification of anti-CVB3 or anti-EV71 inhibitors. The preliminary result suggested that selenenyl sulfides in the present study were effective against CVB3 infection.

### 2.3. Computational chemistry

#### 2.3.1. Proposed binding mode of active compound

Molecular docking has become a useful tool to predict the possible binding mode of inhibitor with biological target, when the co-crystal

**Table 1**

The inhibitions against four 3C/3CL<sup>pro</sup> and cell-based antiviral activities of the target compounds.

Compound	IC <sub>50</sub> (μM) for enzyme inhibition		IC <sub>50</sub> (μM) for cell-based activity	
	EV71-3C <sup>pro</sup>	CVB3-3C <sup>pro</sup>	EV71	CVB3
7a	9.34 ± 0.56	>10	>30	21.2 ± 1.4
7b	2.16 ± 0.42	3.33 ± 0.24	13.4 ± 1.3	10.6 ± 1.1
7c	6.21 ± 0.21	9.64 ± 0.45	25.3 ± 1.1	14.6 ± 1.9
7d	8.79 ± 0.18	9.26 ± 0.53	12.6 ± 0.1	9.27 ± 1.97
7e	>10	>10	18.9 ± 2.1	26.4 ± 2.1
7f	8.72 ± 1.01	9.64 ± 0.27	22.4 ± 0.13	17.8 ± 1.5
7g	9.85 ± 0.11	9.49 ± 0.31	>30	25.4 ± 0.41
7h	>10	>10	>30	>30
7i	3.28 ± 0.47	9.64 ± 0.12	>30	>30
7j	>10	3.26 ± 0.09	16.7 ± 1.3	14.1 ± 1.7
7k	>10	7.69 ± 0.26	24.5 ± 2.1	23.6 ± 1.01
7l	1.78 ± 0.09	3.56 ± 0.21	9.24 ± 0.93	6.58 ± 0.02
7m	>10	9.46 ± 0.12	20.6 ± 2.5	19.1 ± 2.06
7n	>10	>10	16.8 ± 1.6	15.6 ± 0.0
7o	4.31 ± 0.15	3.23 ± 0.03	25.8 ± 2.0	14.6 ± 0.1
7p	2.52 ± 0.20	8.46 ± 0.24	26.8 ± 0.9	14.6 ± 0.2
7q	3.21 ± 0.01	7.62 ± 0.21	9.82 ± 0.7	6.31 ± 0.11
7r	3.28 ± 0.73	2.56 ± 0.09	12.8 ± 0.4	5.42 ± 0.08
7s	6.54 ± 0.37	>10	7.42 ± 1.51	6.21 ± 0.13
7t	2.21 ± 0.06	>10	8.71 ± 0.18	9.62 ± 1.2
7u	>10	>10	20.8 ± 1.8	18.9 ± 2.1
11a	5.18 ± 0.01	2.54 ± 0.01	10.4 ± 0.4	12.4 ± 0.1
11b	5.32 ± 0.22	9.64 ± 0.29	25.7 ± 3.3	11.2 ± 0.2
11c	>10	5.65 ± 0.01	15.7 ± 2.4	24.4 ± 0.2
11d	>10	8.98 ± 0.99	23.9 ± 2.5	13.2 ± 0.2
11e	9.57 ± 0.12	3.01 ± 0.26	5.61 ± 0.21	1.15 ± 0.04
11f	0.28 ± 0.05	1.67 ± 0.31	2.48 ± 0.04	0.72 ± 0.15
11g	2.31 ± 0.11	1.02 ± 0.12	7.28 ± 0.44	5.23 ± 0.11
11h	>10	2.11 ± 0.05	19.4 ± 0.4	16.4 ± 0.6
11i	>10	9.52 ± 0.01	25.1 ± 0.11	13.2 ± 0.3
11j	1.24 ± 0.01	7.99 ± 0.22	>30	>30
11k	7.59 ± 0.24	>10	>30	7.21 ± 1.26
11l	>10	>10	>30	>30
11m	8.21 ± 0.23	3.78 ± 0.05	11.1 ± 1.2	10.4 ± 1.2
11n	>10	9.64 ± 1.76	>30	>30
11o	8.91 ± 0.09	3.46 ± 0.57	>30	25.8 ± 3.01
11p	>10	6.63 ± 0.45	>30	17.9 ± 0.09
11q	3.89 ± 0.04	2.97 ± 0.07	9.59 ± 0.63	14.6 ± 0.8
11r	>10	2.64 ± 0.07	16.0 ± 0.1	22.1 ± 0.2
11s	>10	7.98 ± 0.13	29.9 ± 9.5	>30
11t	9.78 ± 0.11	9.65 ± 0.34	>30	18.2 ± 0.5
11u	2.46 ± 0.78	2.34 ± 0.45	2.35 ± 0.54	5.78 ± 0.11
Rup*	1.03 ± 0.53	2.01 ± 0.22	0.74 ± 0.22	6.52 ± 0.09

\*Rup = rupintrivir.

structure is unavailable (Bondock et al., 2023; Meng et al., 2022; Zhao et al., 2023;). To explore the plausible mode of action for this family of antiviral compounds, **11f** was docked the active site of EV71-3C<sup>pro</sup> (pdb code 3sjo) (Lu et al., 2011). This was because: (i) **11f** was more potent than rupintrivir against EV71-3C<sup>pro</sup>; (ii) Rupintrivir was in the binding pocket of this crystal structure; (iii) EV71-3C<sup>pro</sup> and CVB3-3C<sup>pro</sup> share fairly strong similarity. It should be noted that although this pdb file contained eight chains, these chains were identity in the sequence and the 3D structures superimposed one another perfectly. Therefore we choose chain A for the molecular simulation. Fig. 5a shows the interaction of **11f** and the neighboring residues of EV71-3C<sup>pro</sup> from the molecular simulation in comparison with rupintrivir in the crystal structure. As can be seen, **11f** was much smaller than rupintrivir in size, and **11f** overlaid with the left part of rupintrivir. The selenenyl sulfide inhibitor was involved in multiple hydrophobic contacts with His24, Phe25, His40, Lys143, Ala144, Gly145, His161, Ile162, Gly163, and Gly164, while Gln146 and Cys147 were found to form two hydrogen bonds with **11f**. Fig. 5b depicts the three-dimensional molecular surface of the binding cavity generated by PyMOL and **11f** adopted a relaxed conformation to inhabit in the cavity. Although fewer interactions were observed for **11f** than for rupintrivir with the enzyme, much stronger inhibition of **11f** against EV71 was determined experimentally. We will

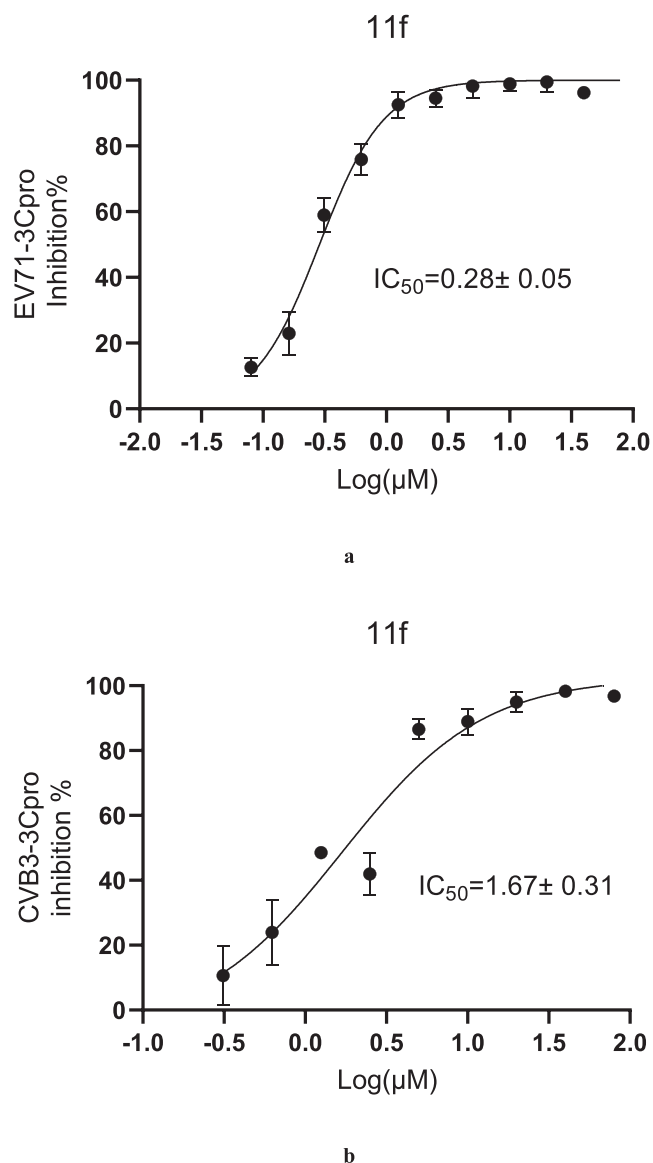


**Fig. 3.** Inhibition curves of **11f** against EV71-3C<sup>pro</sup> (a) and CVB3-3C<sup>pro</sup> (b).

try the co-crystallization of this compound with EV71-3C<sup>pro</sup> or CVB3-3C<sup>pro</sup> to explain the exact mode of action in the future.

### 2.3.2. Structure-activity relationship

Comparative field analysis (CoMFA) is powerful to analyze the quantitative structure-activity relationships (QSAR) of bioactive compounds by steric and electrostatic contributions using three-dimensional models (Cramer et al., 1988). The conformation of **11f** from molecular docking was used to build all the molecular structures. For this study, the cell-based IC<sub>50</sub> values against CVB3 were selected as the biological data to generate the CoMFA model because: (i) There was a bigger training set for building the model; (ii) CoMFA is not limited only to analyze the enzyme inhibitory data. Besides **7h**, **7i**, **11j**, **11l**, **11n** and **11s**, the IC<sub>50</sub> values of which were > 30 μM, compounds **7u**, **11t** and **11u** were also excluded from the training set because they were statistical outliers. The final training set gave a leave-one-out  $q^2$  of 0.519 when the number of optimum components was 6. The non-crossvalidated  $r^2$  was 0.931 with a standard error of estimate of 0.107 and  $F$  values of 18.118. This statistical result indicated that the CoMFA model was successful, even if the compounds belongs to two slightly different series. The steric contribution was 67.3 % and the electrostatic

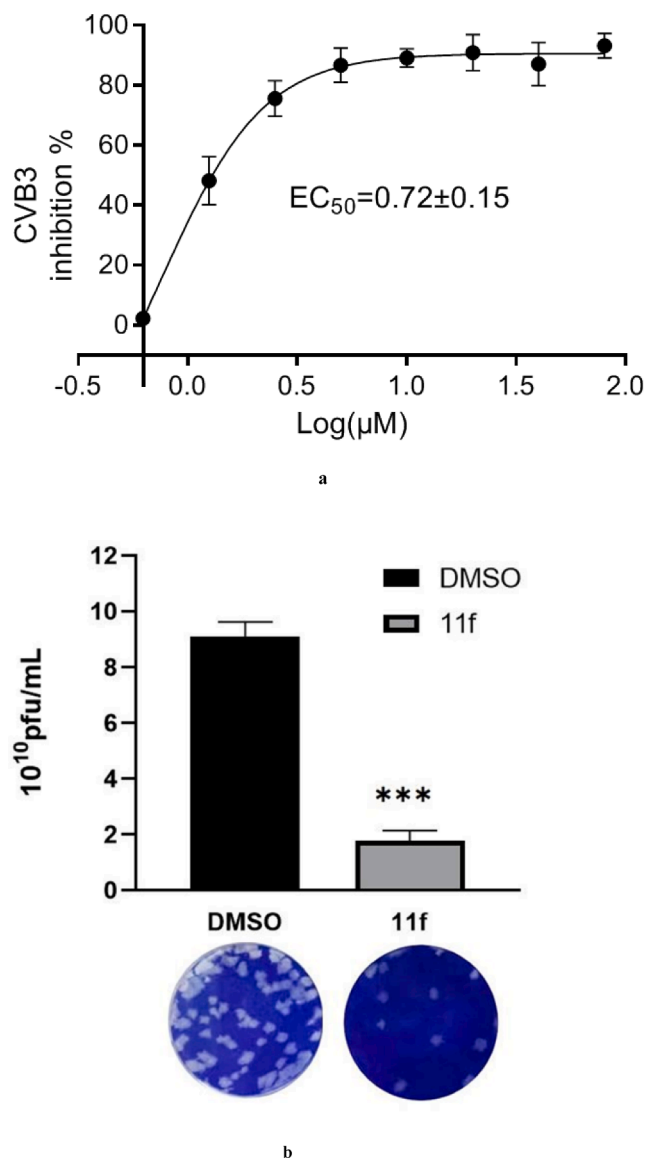


Fig. 4. (a) Inhibition curve of **11f** against CVB3. (b) Anti-CVB3 activity of **11f** from viral plaque assay (the symbol \*\*\* means the significant difference p-value is no more than 0.001).

contribution was 32.7 %. The predicted biological data and experimental biological data from CoMFA were listed in Table 3. The most active compound **11f** was used to explain the contour maps, as shown in Fig. 6. For the steric map (Fig. 6a), a bulky group in the green space is favorable for anti-CVB3 activity, and such a group in the yellow region is likely to decrease the antiviral activity. For the electrostatic map (Fig. 6b), an increase of the positive charge will give enhanced activity in the blue region, whereas in the red space, negatively charged group is likely to improve the cell-based inhibition. Inspired by the above computational chemistry, we will make further structural optimization to seek for compounds with improved activity. For example, it is practical in organic synthesis to introduce a halogen atom at 4-position of the phenyl ring that attached to the sulfur atom of **11f**, and to change the ester moiety to ethyl or propyl group. The next round of molecular design is currently underway.

### 3. Conclusion

In summary, two panels of 42 novel selenenyl sulfides were designed and synthesized via facile nucleophilic substitution reactions, and these

compounds were fully characterized spectroscopically. These selenenyl sulfides were subjected to enzyme inhibitions EV71-3C<sup>Pro</sup> and CVB3-3C<sup>Pro</sup>, and 22 compounds among them displayed IC<sub>50</sub> values below 10 μM against both proteases. The most potent one, being **11f**, exhibited  $0.28 \pm 0.05$  μM IC<sub>50</sub> value against EV71-3C<sup>Pro</sup>, which was sevenfold more effective than that of rupintrivir. For the cell-based antiviral assay, 30 compounds showed IC<sub>50</sub> values below 30 μM against both EV71 and CVB3. Compound **11f** also offered the strongest antiviral activity against CVB3, and that was seven times stronger than rupintrivir. Further cytotoxicity data upon normal Hela cells indicated that **11f** had a relatively high selectivity index of 51.5 against CVB3, and in contrast, rupintrivir only had a selectivity index of 7.6 at the same condition. These results indicated that **11f** is a promising lead compound for further research on antiviral agents targeting 3C<sup>Pro</sup>. In addition, molecular docking was performed to predict a possible binding mode of **11f** with EV71-3C<sup>Pro</sup>, and a CoMFA model was constructed to understand the structure–activity relationships of this class of antiviral compounds. The computational chemistry will provide meaningful guidance for further optimization of this family of inhibitors. For the next step, we will carry out gene knockout experiment to give a direct evidence that the antiviral activity was due to 3C<sup>Pro</sup> inhibition. Moreover, antiviral efficiency will also be evaluated based on an animal model to further investigate the behavior of this compound at a recognized laboratory. In conclusion, this study has brought some exciting results, which is meaningful for the discovery and innovation of novel antiviral inhibitors with different chemical skeletons to combat the risky diseases caused by picornavirus infections.

## 4. Experimental section

### 4.1. Chemistry

The reagents and solvents for the chemical preparation were all of analytical grade quality, purchasing from the online mall for laboratory use in Nankai University ([mall.nankai.edu.cn/labmai/cloudbean](http://mall.nankai.edu.cn/labmai/cloudbean)). All the liquid reagents and organic solvents were dried in advance and distilled using standard methods before use. All the reactions were conducted using oven dried glassware. Melting points were determined using an RT-2 melting apparatus (Shanghai PuZhe photoelectric Co., China) and were uncorrected. <sup>1</sup>H NMR, <sup>13</sup>C NMR, and <sup>77</sup>Se NMR spectra were recorded using a Bruker Avance 400 MHz spectrometer (Bruker Corporation, Switzerland). The chemical shift data ( $\delta$ ) for the nuclear magnetic resonance spectra were expressed as parts per million (ppm), using deuterated chloroform (CDCl<sub>3</sub>) or dimethyl sulfoxide (DMSO-*d*<sub>6</sub>) as solvent and tetramethylsilane (TMS) as an internal standard reference. High-resolution mass spectra were recorded on an FT-ICR mass spectrometer (Ionspec, 7.0 T) or a Varian QFT-ESI instrument (Varian Medical Systems, Crawley, UK). Single crystal X-ray diffraction was carried out on a Bruker Smart 1000 CCD diffractometer (Bruker Corporation, Switzerland). General silica gel (200–300 mesh) was used for the column chromatography purification.

### 4.2. General procedure for synthesis of intermediates and target compounds **7a–7u**

#### 4.2.1. Synthesis of intermediate **2**

To a 25 mL flask, 2-iodobenzoic acid (**1**) (1.24 g, 5 mmol, 1.0 equiv.) was dissolved in freshly distilled thionyl chloride (5 mL) and the reaction mixture was stirred at reflux for 2 h. After that the thionyl chloride was removed via distillation at 100 °C over the course of 1 h and the resulting solid was dried in vacuum to give 2-iodobenzoyl chloride (**2**) in 95 % yield (1.26 g) as a yellow solid without further purification.

#### 4.2.2. Synthesis of intermediate **4**

Phenyl group as R<sup>1</sup> was taken for an example here. To a solution of

**Table 2**  
Cell cytotoxicity against normal Hela cells and selectivity index for anti-CVB3 activity.

Compound	Cell cytotoxicity data (IC <sub>50</sub> , μM)	Selectivity index	Compound	Cell cytotoxicity data (IC <sub>50</sub> , μM)	Selectivity index
7a	125.8 ± 10.4	5.9	11a	100.4 ± 13.8	8.1
7b	106.8 ± 12.5	10.0	11b	99.7 ± 11.0	8.9
7c	111.0 ± 8.8	7.6	11c	126.9 ± 18.7	5.2
7d	51.9 ± 7.3	5.6	11d	81.8 ± 9.9	6.2
7e	118.8 ± 11.4	4.5	11e	27.1 ± 3.2	23.6
7f	87.2 ± 7.8	4.9	11f	37.1 ± 2.5	51.5
7g	81.3 ± 4.6	3.2	11g	35.6 ± 6.2	6.8
7h	N.D.*	N.D.	11h	41.0 ± 5.1	2.5
7i	N.D.	N.D.	11i	99.4 ± 11.4	7.5
7j	173.4 ± 16.5	12.3	11j	N.D.	N.D.
7k	63.7 ± 4.8	2.7	11k	35.3 ± 5.7	4.9
7l	15.1 ± 0.8	2.3	11l	N.D.	N.D.
7m	108.9 ± 18.0	5.7	11m	97.8 ± 13.3	9.4
7n	121.7 ± 17.3	7.8	11n	N.D.	N.D.
7o	110.1 ± 9.9	7.6	11o	38.7 ± 4.7	1.5
7p	156.2 ± 19.3	10.7	11p	35.8 ± 7.5	2.0
7q	41.6 ± 5.8	6.6	11q	99.3 ± 12.0	6.8
7r	50.8 ± 8.1	9.4	11r	99.5 ± 15.4	4.5
7s	50.8 ± 6.1	8.2	11s	N.D.	N.D.
7t	64.5 ± 7.5	6.7	11t	34.6 ± 4.0	1.9
7u	81.2 ± 6.7	4.3	11u	40.5 ± 6.3	7.0
Rup	49.6 ± 5.9	7.6			

\*N.D. = not determined (the IC<sub>50</sub> for the anti-CVB3 data was > 30 μM).

aniline (**3**) (1.24 g, 5 mmol, 1.0 equiv.) and triethylamine (2.1 mL, 15.0 mmol, 3.0 equiv.) was added 2-iodobenzoyl chloride (**2**) (1.06 g, 4 mmol, 0.8 equiv.) in 20 mL dichloromethane dropwise at iced temperature. After 2 h stirring, the mixture was changed to room temperature overnight. When the reaction completed, water (50 mL) was added and the organic layer was separated. The mixture was then washed with 2 mol/L hydrochloric acid (50 mL × 3), saturated sodium bicarbonate (50 mL × 3), and water (50 mL × 3), respectively. Subsequently the organic phase was collected, dried over anhydrous magnesium sulfate, and concentrated under reduced pressure. In the end, the residue was purified by column chromatography (petroleum ether/ethyl acetate = 5/1) to give 2-iodo-*N*-phenylbenzamide (**4**) (1.12 g, 86.7 % yield) as a white solid. The detailed experimental procedures were similar when R<sup>1</sup> was changed to other groups in this study.

#### 4.2.3. Synthesis of intermediate 5

Phenyl group as R<sup>1</sup> was taken for an example here. 1,10-phenanthroline (2.97 g, 16.5 mmol, 3.3 equiv.) and nano copper(I) iodide (2.85 g, 15 mmol, 3 equiv.) were added to *N,N*-dimethylmethanamide (60 mL) and the mixture was stirred for 15 min at room temperature. Subsequently, 2-iodo-*N*-phenylbenzamide (**4**) (4.85 g, 15 mmol, 3 equiv.), selenium powder (1.78 g, 22.5 mmol, 4.5 equiv.), and potassium *t*-butoxide (2.86 g, 25.5 mmol, 5.1 equiv.) were added to the reactant mixture. The reaction was then heated to 110 °C for 12 h under nitrogen atmosphere and after that water (100 mL) was added to quench the reaction. In the next step, the organic phase was extracted with ethyl acetate (100 mL × 3) and the combined ethyl acetate extracts were dried over anhydrous sodium sulfate, filtered, and concentrated under reduced pressure. The intermediate 2-phenylbenzo[d][1,2]selenazol-3(2H)-one (**5**) was purified by column chromatography (petroleum ether/ethyl acetate = 4/1) as a pale-orange solid (2.01 g, 48.7 % yield). The experimental procedures were similar when R<sup>1</sup> was changed to other groups in this study.

All the related intermediates are known compounds and the data for characterization were not provided in this paper (Bhabak and Mughesh, 2007; Dakova et al., 1991; Zhou and Chen, 1999).

#### 4.2.4. Synthesis of target compound 7a-7u

All the substituted thiophenols (2-naphthalenethiol for **7d** and **7n**) were purchased from commercial suppliers. Generally, 1.0 equiv. of **5** was added to 5 mL dichloromethane, after that 1.0 equiv. of different

substituted thiophenol was added to the reactant. The mixture was stirred for 1 h at room temperature and monitored by thin-layer chromatography. The target compound was finally purified by column chromatography (petroleum ether/ethyl acetate = 10/1) in different yields.

4.2.4.1. 2-(((4-fluorophenyl)thio)selanyl)-*N*-phenylbenzamide (**7a**). Pale-yellow solid; Yield 42 %; m.p.: 120–121 °C; <sup>1</sup>H NMR (400 MHz, DMSO-*d*<sub>6</sub>) δ 10.60 (s, 1H, NH), 8.24 (d, *J* = 7.8 Hz, 1H, Ar-H), 8.16 (d, *J* = 8.0 Hz, 1H, Ar-H), 7.74 (d, *J* = 8.4 Hz, 2H, Ar-H), 7.66 (t, *J* = 7.6 Hz, 1H, Ar-H), 7.52 (dq, *J* = 18.0, 7.4, 6.4 Hz, 3H, Ar-H), 7.40 (t, *J* = 7.8 Hz, 2H, Ar-H), 7.17 (q, *J* = 8.2, 7.4 Hz, 3H, Ar-H); <sup>13</sup>C NMR (101 MHz, DMSO-*d*<sub>6</sub>) δ 166.2, 162.5, 160.1, 138.1, 135.7, 132.6, 131.7, 131.3 (d, *J* = 8.3 Hz), 131.0, 128.8, 127.1, 126.4, 124.5, 121.1, 116.2 (d, *J* = 22.2 Hz); <sup>77</sup>Se NMR (76 MHz, DMSO-*d*<sub>6</sub>) δ 615.1; HRMS (ESI) *m/z* calcd for C<sub>19</sub>H<sub>14</sub>FNOSSe [M + H]<sup>+</sup> 404.0018; found 404.0015.

4.2.4.2. 2-(((4-nitrophenyl)thio)selanyl)-*N*-phenylbenzamide (**7b**). Yellow solid; Yield 26 %; m.p. 165–166 °C; <sup>1</sup>H NMR (400 MHz, CDCl<sub>3</sub>) δ 8.19 (d, *J* = 8.9 Hz, 1H, Ar-H), 8.07 (d, *J* = 9.0 Hz, 2H, Ar-H), 8.02 (d, *J* = 7.7 Hz, 1H, Ar-H), 7.78 (d, *J* = 7.3 Hz, 1H, Ar-H), 7.63 (m, 5H, Ar-H), 7.50 (t, *J* = 7.6 Hz, 1H, Ar-H), 7.41 (q, *J* = 8.0 Hz, 3H, Ar-H), 7.23 (t, *J* = 7.4 Hz, 1H, Ar-H); <sup>13</sup>C NMR (101 MHz, CDCl<sub>3</sub>) δ 166.0, 146.1, 136.9, 132.8, 130.9, 129.3, 128.4, 128.1, 126.7 (d, *J* = 3.4 Hz), 126.4, 125.5, 124.5, 123.9, 120.8; <sup>77</sup>Se NMR (76 MHz, CDCl<sub>3</sub>) δ 575.3; HRMS (ESI) *m/z* calcd for C<sub>19</sub>H<sub>14</sub>N<sub>2</sub>O<sub>3</sub>SSe [M - H]<sup>-</sup> 428.9818; found 428.9813.

4.2.4.3. 2-(((2-bromophenyl)thio)selanyl)-*N*-phenylbenzamide (**7c**). White solid; Yield 48 %; m.p. 123–124 °C; <sup>1</sup>H NMR (400 MHz, CDCl<sub>3</sub>) δ 8.04 (d, *J* = 8.2 Hz, 1H, Ar-H), 7.98 (s, 1H, NH), 7.71 (d, *J* = 7.7 Hz, 1H, Ar-H), 7.61 (d, *J* = 7.8 Hz, 2H, Ar-H), 7.55–7.49 (m, 2H, Ar-H), 7.45 (t, *J* = 7.7 Hz, 1H, Ar-H), 7.41–7.28 (m, 3H, Ar-H), 7.16 (m, 2H, Ar-H), 6.98 (td, *J* = 7.8, 1.5 Hz, 1H, Ar-H); <sup>13</sup>C NMR (101 MHz, CDCl<sub>3</sub>) δ 166.1, 139.8, 137.1, 132.7, 132.6, 131.2, 129.7, 129.6, 128.9, 128.1, 127.4, 126.6, 126.4, 125.3, 122.8, 120.7; <sup>77</sup>Se NMR (76 MHz, CDCl<sub>3</sub>) δ 571.2; HRMS (ESI) *m/z* calcd for C<sub>19</sub>H<sub>14</sub>BrNOSSe [M + H]<sup>+</sup> 463.9217; found 463.9213.

4.2.4.4. 2-(((naphthalen-2-ylthio)selanyl)-*N*-phenylbenzamide (**7d**). White solid; Yield 76 %; m.p. 149–150 °C; <sup>1</sup>H NMR (400 MHz,

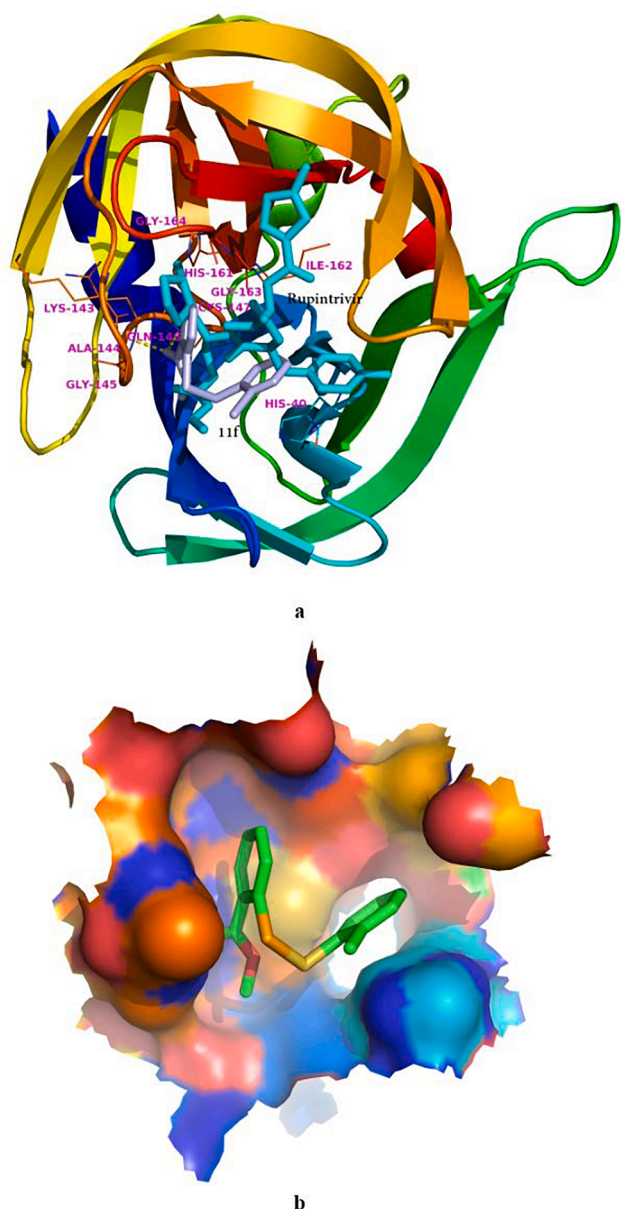


**Fig. 5.** Predicted binding mode of 11f with EV71-3C<sup>Pro</sup>. (a) Comparison of 11f (lightblue) with rupintrivir (cyan), in which the full protein was shown in a cartoon model. (b) The molecular surface of the binding pocket (11f shown in stick model and colored by element).

DMSO-*d*<sub>6</sub>)  $\delta$  10.62 (s, 1H, NH), 8.24 (d, *J* = 7.6 Hz, 1H, Ar-H), 8.17 (d, *J* = 8.1 Hz, 1H, Ar-H), 8.06 (s, 1H, Ar-H), 7.85 (dd, *J* = 13.3, 8.5 Hz, 3H, Ar-H), 7.76 (d, *J* = 7.8 Hz, 2H, Ar-H), 7.62 (t, *J* = 8.1 Hz, 2H, Ar-H), 7.48 (t, *J* = 7.0 Hz, 3H, Ar-H), 7.41 (t, *J* = 7.3 Hz, 2H, Ar-H), 7.18 (t, *J* = 7.2 Hz, 1H, Ar-H); <sup>13</sup>C NMR (101 MHz, DMSO-*d*<sub>6</sub>)  $\delta$  166.3, 138.1, 135.9, 133.2, 133.0, 132.5, 131.6, 131.1, 128.9, 128.8, 128.7, 127.7, 127.3, 127.08, 127.03, 126.8, 126.4, 126.1, 124.5, 121.1; <sup>77</sup>Se NMR (76 MHz, DMSO-*d*<sub>6</sub>)  $\delta$  590.0; HRMS (ESI) *m/z* calcd for C<sub>23</sub>H<sub>17</sub>NOSse [M + H]<sup>+</sup> 436.0269; found 436.0268.

**4.2.4.5. *N*-benzyl-2-(((4-fluorophenyl)thio)selanyl)benzamide (7e).** White solid; Yield 20 %; m.p. 111–112 °C; <sup>1</sup>H NMR (400 MHz, CDCl<sub>3</sub>)  $\delta$  8.25 (d, *J* = 8.1 Hz, 1H, Ar-H), 7.57 (d, *J* = 7.7 Hz, 1H, Ar-H), 7.50 (q, *J* = 7.0, 6.1 Hz, 3H, Ar-H), 7.35 (d, *J* = 5.9 Hz, 5H, Ar-H), 7.26 (t, *J* = 7.5 Hz, 1H, Ar-H), 6.94 (t, *J* = 8.7 Hz, 2H, Ar-H), 6.71 (s, 1H, NH), 4.66 (d, *J* = 5.6 Hz, 2H, CH<sub>2</sub>); <sup>13</sup>C NMR (101 MHz, CDCl<sub>3</sub>)  $\delta$  167.7, 163.2, 160.7,

**Table 3**

Predicted biological data versus experimental biological data from CoMFA.

Compound	ED	PD	ER	Compound	ED	PD	ER
7a	4.77	4.58	0.19	7t	5.02	4.97	0.05
7b	4.97	5.06	-0.09	11a	4.91	5.02	-0.11
7c	4.83	4.86	-0.03	11b	4.95	4.81	0.14
7d	5.03	5.00	0.03	11c	4.61	4.80	-0.19
7e	4.58	4.70	-0.12	11d	4.88	4.73	0.15
7f	4.75	4.65	0.10	11e	5.94	5.99	-0.05
7g	4.60	4.58	0.02	11f	6.14	6.15	-0.01
7j	4.85	4.82	0.03	11g	5.28	5.21	0.07
7k	4.63	4.65	-0.02	11h	4.78	4.83	-0.05
7l	5.18	5.22	-0.04	11i	4.88	4.89	-0.01
7m	4.72	4.75	-0.03	11k	5.14	5.38	-0.24
7n	4.80	4.82	-0.02	11m	4.98	4.90	0.08
7o	4.83	4.92	-0.09	11o	4.58	4.65	-0.07
7p	4.84	4.85	-0.01	11p	4.75	4.78	-0.03
7q	5.20	5.18	0.02	11q	4.84	4.93	-0.09
7r	5.27	5.19	0.08	11r	4.66	4.54	0.12
7s	5.20	5.14	0.06	11t	4.74	4.54	0.20

\*ED = experimental pIC<sub>50</sub> data, PD = predicted pIC<sub>50</sub> data, ER = error.

137.5, 137.3, 132.2, 131.3 (d, *J* = 8.0 Hz), 130.5, 128.9, 128.3, 128.0, 127.9, 126.6, 126.1, 115.9 (d, *J* = 22.0 Hz), 44.3; <sup>77</sup>Se NMR (76 MHz, CDCl<sub>3</sub>)  $\delta$  616.8; HRMS (ESI) *m/z* calcd for C<sub>20</sub>H<sub>16</sub>FNOsse [M + Na]<sup>+</sup> 439.9994; found 439.9998.

**4.2.4.6. *N*-benzyl-2-(((4-bromophenyl)thio)selanyl)benzamide (7f).** White solid; Yield 19 %; m.p. 135–136 °C; <sup>1</sup>H NMR (400 MHz, CDCl<sub>3</sub>)  $\delta$  8.13 (d, *J* = 8.1 Hz, 1H, Ar-H), 7.54 (d, *J* = 7.7 Hz, 1H, Ar-H), 7.46 (t, *J* = 7.0 Hz, 1H, Ar-H), 7.40–7.31 (m, 9H, Ar-H), 7.27 (t, *J* = 8.0 Hz, 1H, Ar-H), 6.53 (s, 1H, NH), 4.68 (d, *J* = 5.6 Hz, 2H, CH<sub>2</sub>); <sup>13</sup>C NMR (101 MHz, CDCl<sub>3</sub>)  $\delta$  167.6, 137.4, 137.2, 136.1, 132.3, 131.8, 130.4, 128.9, 128.4, 128.1, 126.4, 126.1, 120.2, 44.4; <sup>77</sup>Se NMR (76 MHz, CDCl<sub>3</sub>)  $\delta$  597.0; HRMS (ESI) *m/z* calcd for C<sub>20</sub>H<sub>16</sub>BrNOsse [M + H]<sup>+</sup> 477.9374; found 477.9368.

**4.2.4.7. *N*-benzyl-2-(((2-bromophenyl)thio)selanyl)benzamide (7g).** Pale-yellow solid; Yield 7 %; m.p. 135–136 °C; <sup>1</sup>H NMR (400 MHz, CDCl<sub>3</sub>)  $\delta$  8.13 (d, *J* = 8.1 Hz, 1H, Ar-H), 7.54 (d, *J* = 7.7 Hz, 1H, Ar-H), 7.46 (t, *J* = 7.0 Hz, 1H, Ar-H), 7.40–7.31 (m, 9H, Ar-H), 7.27 (t, *J* = 8.0 Hz, 1H, Ar-H), 6.53 (s, 1H, NH), 4.68 (d, *J* = 5.6 Hz, 2H, CH<sub>2</sub>); <sup>13</sup>C NMR (101 MHz, CDCl<sub>3</sub>)  $\delta$  167.7, 137.4, 137.2, 136.9, 132.7, 132.4, 130.5, 129.6, 128.9, 128.7, 128.1, 128.0, 127.9, 127.3, 126.4, 126.2, 122.7, 44.4, 29.7; <sup>77</sup>Se NMR (76 MHz, CDCl<sub>3</sub>)  $\delta$  566.7; HRMS (ESI) *m/z* calcd for C<sub>20</sub>H<sub>16</sub>BrNOsse [M + H]<sup>+</sup> 477.9374; found 477.9370.

**4.2.4.8. *N*-benzyl-2-(((3-(trifluoromethyl)phenyl)thio)selanyl)benzamide (7h).** Pale-yellow solid; Yield 28 %; m.p. 100–101 °C; <sup>1</sup>H NMR (400 MHz, CDCl<sub>3</sub>)  $\delta$  8.12 (d, *J* = 8.1 Hz, 1H, Ar-H), 7.76 (s, 1H, Ar-H), 7.68 (d, *J* = 7.7 Hz, 1H, Ar-H), 7.55 (d, *J* = 7.8 Hz, 1H, Ar-H), 7.49–7.43 (m, 1H, Ar-H), 7.41–7.27 (m, 8H, Ar-H), 6.56 (s, 1H, NH), 4.69 (d, *J* = 5.6 Hz, 2H, CH<sub>2</sub>); <sup>13</sup>C NMR (101 MHz, CDCl<sub>3</sub>)  $\delta$  167.7, 138.4, 137.4, 136.9, 132.4, 131.9, 130.4, 129.3, 128.9, 128.2, 128.0, 127.9, 126.5, 126.2, 125.3 (q, *J* = 4.0 Hz), 125.3, 125.2, 123.0 (d, *J* = 3.7 Hz), 44.4; <sup>77</sup>Se NMR (76 MHz, CDCl<sub>3</sub>)  $\delta$  590.4; HRMS (ESI) *m/z* calcd for C<sub>21</sub>H<sub>16</sub>F<sub>3</sub>NOsse [M + H]<sup>+</sup> 468.0143; found 468.0147.

**4.2.4.9. 2-(((4-chlorophenyl)thio)selanyl)-*N*-(4-methoxyphenyl)benzamide (7i).** White solid; Yield 75 %; m.p. 148–149 °C; <sup>1</sup>H NMR (400 MHz, CDCl<sub>3</sub>)  $\delta$  8.17 (d, *J* = 8.1 Hz, 1H, Ar-H), 7.89 (s, 1H, NH), 7.70 (d, *J* = 7.6 Hz, 1H, Ar-H), 7.49 (t, *J* = 7.6 Hz, 3H, Ar-H), 7.43 (d, *J* = 8.2 Hz, 2H, Ar-H), 7.34 (t, *J* = 7.4 Hz, 1H, Ar-H), 7.18 (d, *J* = 8.4 Hz, 2H, Ar-H), 6.92 (d, *J* = 8.5 Hz, 2H, Ar-H), 3.82 (s, 3H, OCH<sub>3</sub>); <sup>13</sup>C NMR (101 MHz, CDCl<sub>3</sub>)  $\delta$  165.9, 157.2, 137.3, 135.3, 132.4, 131.1, 130.2, 130.0, 128.9, 128.6, 126.5, 126.3, 122.7, 114.4, 55.6; <sup>77</sup>Se NMR (76 MHz, CDCl<sub>3</sub>)  $\delta$  599.0; HRMS (ESI) *m/z* calcd for C<sub>20</sub>H<sub>16</sub>ClNO<sub>2</sub>Se [M + H]<sup>+</sup> 449.9828;

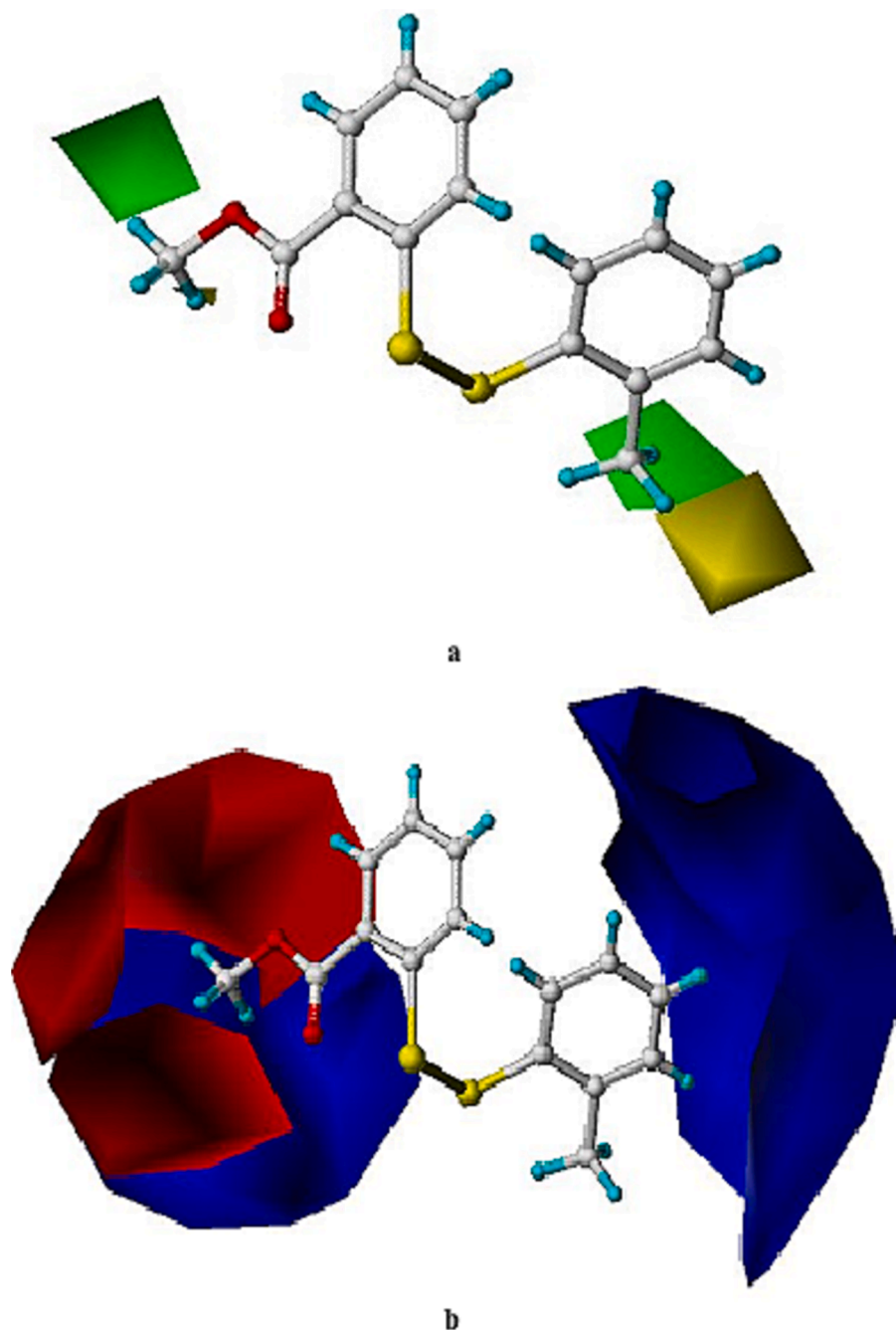


**Fig. 6.** Three-dimensional contour maps of the anti-CVB3 activities from the CoMFA model for (a) steric field and (b) electrostatic field contributions.

found 449.9827.

**4.2.4.10.** *2-(((4-bromophenyl)thio)selanyl)-N-(4-methoxyphenyl)benzamide (7j)*. White solid; Yield 79 %; m.p. 149–150 °C;  $^1\text{H}$  NMR (400 MHz,  $\text{CDCl}_3$ )  $\delta$  8.16 (d,  $J = 8.1$  Hz, 1H, Ar-H), 7.87 (s, 1H, NH), 7.70 (d,  $J = 7.6$  Hz, 1H, Ar-H), 7.50 (t,  $J = 8.8$  Hz, 3H, Ar-H), 7.36 (q,  $J = 8.4$  Hz, 5H, Ar-H), 6.93 (d,  $J = 8.4$  Hz, 2H, Ar-H), 3.83 (s, 3H,  $\text{OCH}_3$ );  $^{13}\text{C}$  NMR (101 MHz,  $\text{CDCl}_3$ )  $\delta$  165.9, 157.2, 137.3, 135.9, 132.4, 131.9, 131.1, 130.4, 130.0, 128.6, 126.5, 126.2, 122.7, 120.2, 114.4, 55.5;  $^{77}\text{Se}$  NMR (76 MHz,  $\text{CDCl}_3$ )  $\delta$  597.8; HRMS (ESI)  $m/z$  calcd for  $\text{C}_{20}\text{H}_{16}\text{BrNO}_2\text{SSe}$   $[\text{M} + \text{H}]^+$  493.9323, found 493.9318.

**4.2.4.11.** *N-(4-methoxyphenyl)-2-(((4-methoxyphenyl)thio)selanyl)benzamide (7k)*. White solid; Yield 67 %; m.p. 129–130 °C;  $^1\text{H}$  NMR (400 MHz,  $\text{CDCl}_3$ )  $\delta$  8.33 (d,  $J = 8.1$  Hz, 1H, Ar-H), 7.81 (s, 1H, NH), 7.64 (d,

$J = 7.7$  Hz, 1H, Ar-H), 7.54–7.40 (m, 5H, Ar-H), 7.29 (t,  $J = 7.5$  Hz, 1H, Ar-H), 6.88 (d,  $J = 9.0$  Hz, 2H, Ar-H), 6.75 (d,  $J = 8.8$  Hz, 2H, Ar-H), 3.79 (s, 3H,  $\text{OCH}_3$ ), 3.73 (s, 3H,  $\text{OCH}_3$ );  $^{13}\text{C}$  NMR (101 MHz,  $\text{CDCl}_3$ )  $\delta$  165.9, 159.1, 157.0, 137.6, 132.1, 132.0, 131.4, 130.1, 128.9, 127.7, 126.6, 126.1, 122.5, 114.6, 114.3, 55.5, 55.3;  $^{77}\text{Se}$  NMR (76 MHz,  $\text{CDCl}_3$ )  $\delta$  633.7; HRMS (ESI)  $m/z$  calcd for  $\text{C}_{21}\text{H}_{19}\text{NO}_3\text{SSe}$   $[\text{M} + \text{H}]^+$  446.0324; found 446.0326.

**4.2.4.12.** *N-(4-methoxyphenyl)-2-(((4-nitrophenyl)thio)selanyl)benzamide (7l)*. Yellow solid; Yield 85 %; m.p. 189–190 °C.  $^1\text{H}$  NMR (400 MHz,  $\text{DMSO}-d_6$ )  $\delta$  8.05 (d,  $J = 9.0$  Hz, 2H, Ar-H), 8.00 (d,  $J = 8.9$  Hz, 1H, Ar-H), 7.92 (s, 1H, NH), 7.73 (d,  $J = 7.5$  Hz, 1H, Ar-H), 7.60 (d,  $J = 9.0$  Hz, 2H, Ar-H), 7.51 (d,  $J = 9.0$  Hz, 2H, Ar-H), 7.49–7.44 (m, 1H, Ar-H), 7.37 (t,  $J = 7.9$  Hz, 1H, Ar-H), 6.93 (d,  $J = 9.0$  Hz, 2H, Ar-H), 3.81 (s, 3H,  $\text{OCH}_3$ );  $^{13}\text{C}$  NMR (101 MHz,  $\text{DMSO}-d_6$ )  $\delta$  166.0, 156.3, 145.6, 135.2,

132.8, 130.9, 128.9, 128.2, 126.9, 126.7, 124.5, 124.1, 123.0, 122.2, 113.9, 55.2;  $^{77}\text{Se}$  NMR (76 MHz, DMSO- $d_6$ )  $\delta$  577.3; HRMS (ESI)  $m/z$  calcd for  $\text{C}_{20}\text{H}_{16}\text{N}_2\text{O}_4\text{SSe}$   $[\text{M}-\text{H}]^-$  458.9923; found 458.9920.

4.2.4.13. *2-(((2-bromophenyl)thio)selanyl)-N-(4-methoxyphenyl)benzamide (7m)*. Pale-yellow solid; Yield 57 %; m.p. 154–155 °C;  $^1\text{H}$  NMR (400 MHz,  $\text{CDCl}_3$ )  $\delta$  8.05 (d,  $J = 8.0$  Hz, 1H, Ar-H), 7.92 (s, 1H, NH), 7.71 (d,  $J = 7.6$  Hz, 1H, Ar-H), 7.52 (q,  $J = 10.2, 9.3$  Hz, 4H, Ar-H), 7.46 (d,  $J = 7.6$  Hz, 1H, Ar-H), 7.34 (t,  $J = 7.3$  Hz, 1H, Ar-H), 7.16 (t,  $J = 7.5$  Hz, 1H, Ar-H), 7.00 (t,  $J = 7.5$  Hz, 1H, Ar-H), 6.93 (d,  $J = 8.5$  Hz, 2H, Ar-H), 3.82 (s, 3H,  $\text{OCH}_3$ );  $^{13}\text{C}$  NMR (101 MHz,  $\text{CDCl}_3$ )  $\delta$  166.0, 157.2, 137.1, 132.7, 132.5, 131.2, 129.9, 129.6, 128.9, 128.1, 127.4, 126.4, 126.3, 122.7, 114.4, 55.6;  $^{77}\text{Se}$  NMR (76 MHz,  $\text{CDCl}_3$ )  $\delta$  573.1; HRMS (ESI)  $m/z$  calcd for  $\text{C}_{20}\text{H}_{16}\text{BrNO}_2\text{SSe}$   $[\text{M} + \text{H}]^+$  493.9323; found 493.9323.

4.2.4.14. *N-(4-fluorophenyl)-2-((naphthalen-2-ylthio)selanyl)benzamide (7n)*. White solid; Yield 27 %; m.p. 154–155 °C;  $^1\text{H}$  NMR (400 MHz,  $\text{CDCl}_3$ )  $\delta$  8.30 (d,  $J = 8.2$  Hz, 1H, Ar-H), 8.00 (s, 1H, Ar-H), 7.94 (s, 1H, NH), 7.79 (d,  $J = 7.8$  Hz, 1H, Ar-H), 7.73 (t,  $J = 7.1$  Hz, 3H, Ar-H), 7.62 (m, 3H, Ar-H), 7.47 (m, 3H, Ar-H), 7.36 (t,  $J = 7.5$  Hz, 1H, Ar-H), 7.12 (t,  $J = 8.2$  Hz, 2H, Ar-H);  $^{13}\text{C}$  NMR (101 MHz,  $\text{CDCl}_3$ )  $\delta$  166.1, 161.1, 158.7, 137.8, 133.7 (d,  $J = 15.3$  Hz), 133.1 (d,  $J = 2.7$  Hz), 132.5, 132.2, 131.1, 129.0, 128.6, 127.7, 127.4, 127.4, 127.1, 126.6 (d,  $J = 3.8$  Hz), 126.2, 125.9, 122.7 (d,  $J = 8.0$  Hz), 116.0, 115.8;  $^{77}\text{Se}$  NMR (76 MHz,  $\text{CDCl}_3$ )  $\delta$  590.4; HRMS (ESI)  $m/z$  calcd for  $\text{C}_{23}\text{H}_{16}\text{FNO}_2\text{SSe}$   $[\text{M}-\text{H}]^-$  452.0029; found 452.0023.

4.2.4.15. *2-(((2-bromophenyl)thio)selanyl)-N-(4-chlorophenyl)benzamide (7o)*. White solid; Yield 57 %; m.p. 159–160 °C;  $^1\text{H}$  NMR (400 MHz, DMSO- $d_6$ )  $\delta$  10.67 (s, 1H, NH), 8.25 (d,  $J = 7.7$  Hz, 1H, Ar-H), 8.06 (d,  $J = 8.1$  Hz, 1H, Ar-H), 7.80–7.71 (m, 3H, Ar-H), 7.64 (t,  $J = 7.6$  Hz, 2H, Ar-H), 7.55–7.39 (m, 6H, Ar-H), 7.25 (t,  $J = 8.8$  Hz, 3H, Ar-H);  $^{13}\text{C}$  NMR (101 MHz, DMSO- $d_6$ )  $\delta$  166.7, 160.5, 158.1, 136.0, 134.9, 133.2, 132.5, 131.3, 131.1, 129.4, 127.6, 127.0, 123.6 (d,  $J = 8.0$  Hz), 120.2, 115.9 (d,  $J = 22.3$  Hz);  $^{77}\text{Se}$  NMR (76 MHz, DMSO- $d_6$ )  $\delta$  594.9; HRMS (ESI)  $m/z$  calcd for  $\text{C}_{19}\text{H}_{13}\text{BrClNO}_2\text{SSe}$   $[\text{M}-\text{H}]^-$  495.8682; found 495.8673.

4.2.4.16. *2-(((2-bromophenyl)thio)selanyl)-N-(4-chlorophenyl)benzamide (7p)*. White solid; Yield 22 %; m.p. 163–164 °C;  $^1\text{H}$  NMR (400 MHz,  $\text{CDCl}_3$ )  $\delta$  8.07 (d,  $J = 8.1$  Hz, 1H, Ar-H), 7.96 (s, 1H, NH), 7.71 (d,  $J = 7.6$  Hz, 1H, Ar-H), 7.59 (d,  $J = 8.8$  Hz, 2H, Ar-H), 7.53 (ddd,  $J = 7.9, 4.4, 1.4$  Hz, 2H, Ar-H), 7.49 (t,  $J = 7.7$  Hz, 1H, Ar-H), 7.36 (d,  $J = 8.7$  Hz, 3H, Ar-H), 7.16 (t,  $J = 7.6$  Hz, 1H, Ar-H), 7.01 (t,  $J = 7.6$  Hz, 1H, Ar-H);  $^{13}\text{C}$  NMR (101 MHz,  $\text{CDCl}_3$ )  $\delta$  166.0, 137.2, 136.9, 135.6, 132.8 (d,  $J = 6.4$  Hz), 130.9, 130.4, 129.7, 129.3, 129.1, 128.1, 127.5, 126.7, 126.4, 122.8, 121.9;  $^{77}\text{Se}$  NMR (76 MHz,  $\text{CDCl}_3$ )  $\delta$  571.2; HRMS (ESI)  $m/z$  calcd for  $\text{C}_{19}\text{H}_{13}\text{BrClNO}_2\text{SSe}$   $[\text{M} + \text{H}]^+$  497.8828; found 497.8821.

4.2.4.17. *N-(4-chlorophenyl)-2-(((2-methoxyphenyl)thio)selanyl)benzamide (7q)*. White solid; Yield 55 %; m.p. 287–288 °C;  $^1\text{H}$  NMR (400 MHz,  $\text{CDCl}_3$ )  $\delta$  8.20 (d,  $J = 8.1$  Hz, 1H, Ar-H), 7.94 (s, 1H, NH), 7.66 (d,  $J = 7.6$  Hz, 1H, Ar-H), 7.55 (d,  $J = 8.7$  Hz, 2H, Ar-H), 7.48–7.42 (m, 2H, Ar-H), 7.30 (dd,  $J = 15.1, 8.0$  Hz, 3H, Ar-H), 7.18–7.12 (m, 1H, Ar-H), 6.81 (m, 2H, Ar-H), 3.88 (s, 3H,  $\text{OCH}_3$ );  $^{13}\text{C}$  NMR (101 MHz,  $\text{CDCl}_3$ )  $\delta$  166.1, 157.4, 137.7, 135.8, 132.4, 131.3, 130.7, 130.2, 129.5, 128.1, 127.8, 126.5, 126.1, 121.8, 121.3, 110.6, 55.9;  $^{77}\text{Se}$  NMR (76 MHz,  $\text{CDCl}_3$ )  $\delta$  561.6; HRMS (ESI)  $m/z$  calcd for  $\text{C}_{20}\text{H}_{16}\text{ClNO}_2\text{SSe}$   $[\text{M} + \text{H}]^+$  449.9828; found 449.9835.

4.2.4.18. *N-(4-bromophenyl)-2-(((4-fluorophenyl)thio)selanyl)benzamide (7r)*. White solid; Yield 20 %; m.p. 161–162 °C;  $^1\text{H}$  NMR (400 MHz,  $\text{CDCl}_3$ )  $\delta$  8.30 (d,  $J = 8.8$  Hz, 1H, Ar-H), 7.92 (s, 1H, NH), 7.72 (d,  $J = 8.8$  Hz, 1H, Ar-H), 7.59–7.48 (m, 7H, Ar-H), 7.39 (t,  $J = 7.4$  Hz, 1H, Ar-

H), 6.95 (t,  $J = 8.7$  Hz, 2H, Ar-H);  $^{13}\text{C}$  NMR (101 MHz,  $\text{CDCl}_3$ )  $\delta$  166.0, 163.3, 160.8, 137.6, 136.2, 132.6, 132.2, 131.5, 131.4, 130.9, 128.8, 126.8, 126.3, 122.2, 117.9, 116.1, 115.9;  $^{77}\text{Se}$  NMR (76 MHz,  $\text{CDCl}_3$ )  $\delta$  615.0; HRMS (ESI)  $m/z$  calcd for  $\text{C}_{19}\text{H}_{13}\text{BrFNO}_2\text{SSe}$   $[\text{M} + \text{H}]^+$  481.9123; found 481.9115.

4.2.4.19. *N-(4-bromophenyl)-2-(((4-bromophenyl)thio)selanyl)benzamide (7s)*. White solid; Yield 37 %; m.p. 284–285 °C;  $^1\text{H}$  NMR (400 MHz,  $\text{CDCl}_3$ )  $\delta$  8.18 (d,  $J = 8.9$  Hz, 1H, Ar-H), 7.91 (s, 1H, NH), 7.70 (d,  $J = 7.7$  Hz, 1H, Ar-H), 7.56–7.48 (m, 5H, Ar-H), 7.35 (m, 5H, Ar-H);  $^{13}\text{C}$  NMR (101 MHz,  $\text{CDCl}_3$ )  $\delta$  166.0, 137.5, 136.2, 135.8, 132.7, 132.2, 131.9, 130.8, 130.6, 129.4, 128.8, 126.6, 126.4, 122.1, 120.4, 118.0;  $^{77}\text{Se}$  NMR (76 MHz,  $\text{CDCl}_3$ )  $\delta$  598.6; HRMS (ESI)  $m/z$  calcd for  $\text{C}_{19}\text{H}_{13}\text{Br}_2\text{NO}_2\text{SSe}$   $[\text{M}-\text{H}]^-$  539.8177; found 539.8170.

4.2.4.20. *N-(4-bromophenyl)-2-(((4-methoxyphenyl)thio)selanyl)benzamide (7t)*. White solid; Yield 14 %; m.p. 112–113 °C;  $^1\text{H}$  NMR (400 MHz,  $\text{CDCl}_3$ )  $\delta$  8.35 (d,  $J = 8.1$  Hz, 1H, Ar-H), 7.94 (s, 1H, NH), 7.67 (d,  $J = 7.7$  Hz, 1H, Ar-H), 7.55–7.43 (m, 7H, Ar-H), 7.31 (t,  $J = 7.4$  Hz, 1H, Ar-H), 6.77 (dd,  $J = 8.7, 1.9$  Hz, 2H, Ar-H), 3.74 (d,  $J = 2.0$  Hz, 3H,  $\text{OCH}_3$ );  $^{13}\text{C}$  NMR (101 MHz,  $\text{CDCl}_3$ )  $\delta$  166.0, 159.3, 137.3, 136.4, 132.4, 132.1, 131.2, 129.2, 127.6, 126.7, 126.2, 122.1, 117.8, 114.6, 55.4;  $^{77}\text{Se}$  NMR (76 MHz,  $\text{CDCl}_3$ )  $\delta$  633.2; HRMS (ESI)  $m/z$  calcd for  $\text{C}_{20}\text{H}_{16}\text{BrNO}_2\text{SSe}$   $[\text{M}-\text{H}]^-$  491.9178; found 491.9170.

4.2.4.21. *N-(4-bromophenyl)-2-(((4-methoxyphenyl)thio)selanyl)benzamide (7u)*. Yellow solid; Yield 69 %; m.p. 190–191 °C;  $^1\text{H}$  NMR (400 MHz, DMSO- $d_6$ )  $\delta$  8.06 (d,  $J = 8.9$  Hz, 2H, Ar-H), 8.01 (d,  $J = 8.2$  Hz, 1H, Ar-H), 7.95 (s, 1H, NH), 7.74 (d,  $J = 7.8$  Hz, 1H, Ar-H), 7.60 (d,  $J = 8.9$  Hz, 2H, Ar-H), 7.51 (dd,  $J = 12.2, 2.9$  Hz, 5H, Ar-H), 7.38 (t,  $J = 7.1$  Hz, 1H, Ar-H);  $^{13}\text{C}$  NMR (101 MHz, DMSO- $d_6$ )  $\delta$  167.0, 146.1, 145.9, 137.9, 135.8, 133.6, 132.1, 131.2, 129.6, 128.7, 127.5, 127.2, 124.6, 123.6, 122.9, 117.0;  $^{77}\text{Se}$  NMR (76 MHz, DMSO- $d_6$ )  $\delta$  574.9; HRMS (ESI)  $m/z$  calcd for  $\text{C}_{19}\text{H}_{13}\text{BrN}_2\text{O}_3\text{SSe}$   $[\text{M} + \text{H}]^+$  508.9068; found 508.9059.

### 4.3. General procedure for synthesis of intermediates and target compounds 11a–11u

#### 4.3.1. Synthesis of intermediate 9 and 10

Methyl group as  $\text{R}^3$  was taken for an example here. Methyl 2-aminobenzoate (3.02 g, 20 mmol, 4 equiv.) was added to a 250 mL round flask, hydrochloric acid (2 M, 12 mL) was then added slowly to the flask at ice bath condition. Under stirring, sodium nitrite solution (3 M, 8 mL) was added until the solution became transparent and clear. Subsequently, saturated sodium acetate was added to adjust the pH value to 4.8 and the temperature was changed to room temperature. The intermediate 9 was not separated since it was a diazo salt. Subsequently, potassium selenocyanate (2.88 g, 20 mmol, 4 equiv.) was added to the mixture when bubbles produced and orange solid precipitated. The reaction completed when no more bubbles came out. The product was filtered to give orange solid methyl 2-selenocyanatobenzoate (10) in 81.5 % yield.

The synthesis was in a similar manner when  $\text{R}^3$  was ethyl. These intermediates were known compounds and have not been characterized in this paper (Alberto et al., 2012; Jones et al., 2002; Dakova et al., 1991).

#### 4.3.2. Synthesis of target compound 11a–11u

All the substituted thiophenols (2-naphthalenethiol for 11l and 11u) were from the same commercial sources as those for the synthesis of 7a–7u. Generally, 1.0 equiv. of intermediate 10 was added to 5 mL dichloromethane, after that 1.0 equiv. of different substituted thiophenol and catalytic amount of aluminum oxide was added to the reactant. The mixture was stirred for 30 min at room temperature and monitored by thin-layer chromatography. The target compound was finally purified by column chromatography (n-hexane/ethyl acetate = 100/1) in different yields.

**4.3.2.1. Methyl 2-((*p*-tolylthio)selanyl)benzoate (11a).** White solid; Yield 53 %; m.p. 51–52 °C;  $^1\text{H}$  NMR (400 MHz,  $\text{CDCl}_3$ )  $\delta$  8.20 (d,  $J = 8.7$  Hz, 1H, Ar-H), 8.04 (dd,  $J = 7.8, 1.4$  Hz, 1H, Ar-H), 7.53–7.47 (m, 1H, Ar-H), 7.38 (d,  $J = 8.2$  Hz, 2H, Ar-H), 7.27 (t,  $J = 7.0$  Hz, 1H, Ar-H), 7.02 (d,  $J = 8.1$  Hz, 2H, Ar-H), 3.95 (s, 3H,  $\text{OCH}_3$ ), 2.27 (s, 3H,  $\text{CH}_3$ );  $^{13}\text{C}$  NMR (101 MHz,  $\text{CDCl}_3$ )  $\delta$  168.0, 138.6, 136.8, 133.4, 132.9, 131.3, 129.7, 129.4, 127.5, 127.1, 125.9, 52.7, 20.9;  $^{77}\text{Se}$  NMR (76 MHz,  $\text{CDCl}_3$ )  $\delta$  602.9; HRMS (ESI)  $m/z$  calcd for  $\text{C}_{15}\text{H}_{14}\text{O}_2\text{SSe}$  [ $\text{M} + \text{Na}$ ] $^+$  360.9772; found 360.9775.

**4.3.2.2. Methyl 2-(((4-fluorophenyl)thio)selanyl)benzoate (11b).** White solid; Yield 14 %; m.p. 68–69 °C;  $^1\text{H}$  NMR (400 MHz,  $\text{CDCl}_3$ )  $\delta$  8.18 (d,  $J = 8.3$  Hz, 1H, Ar-H), 8.05 (d,  $J = 9.2$  Hz, 1H, Ar-H), 7.52 (t,  $J = 8.4$  Hz, 1H, Ar-H), 7.45 (dd,  $J = 8.8, 5.1$  Hz, 2H, Ar-H), 7.29 (t,  $J = 7.5$  Hz, 1H, Ar-H), 6.91 (t,  $J = 8.7$  Hz, 2H, Ar-H), 3.96 (s, 3H,  $\text{OCH}_3$ );  $^{13}\text{C}$  NMR (101 MHz,  $\text{CDCl}_3$ )  $\delta$  168.1, 163.3, 160.8, 138.2, 133.5, 131.4, 131.3, 131.3, 127.3, 127.1, 126.1, 116.1, 115.9, 52.7;  $^{77}\text{Se}$  NMR (76 MHz,  $\text{CDCl}_3$ )  $\delta$  615.7; HRMS (ESI)  $m/z$  calcd for  $\text{C}_{14}\text{H}_{11}\text{FO}_2\text{SSe}$  [ $\text{M} + \text{Na}$ ] $^+$  364.9521; found 364.9518.

**4.3.2.3. Methyl 2-(((4-chlorophenyl)thio)selanyl)benzoate (11c).** Yellow solid; Yield 46 %; m.p. 72–73 °C;  $^1\text{H}$  NMR (400 MHz,  $\text{CDCl}_3$ )  $\delta$  8.09 (d,  $J = 8.2$  Hz, 1H, Ar-H), 8.06 (dd,  $J = 7.8, 1.3$  Hz, 1H, Ar-H), 7.53–7.47 (m, 1H, Ar-H), 7.40 (d,  $J = 8.6$  Hz, 2H, Ar-H), 7.29 (t,  $J = 7.5$  Hz, 1H, Ar-H), 7.17 (d,  $J = 8.6$  Hz, 2H, Ar-H), 3.97 (s, 3H,  $\text{OCH}_3$ );  $^{13}\text{C}$  NMR (101 MHz,  $\text{CDCl}_3$ )  $\delta$  168.1, 138.0, 134.9, 133.6, 132.6, 130.2, 129.0, 127.3, 127.2, 126.1, 52.9;  $^{77}\text{Se}$  NMR (76 MHz,  $\text{CDCl}_3$ )  $\delta$  597.0; HRMS (ESI)  $m/z$  calcd for  $\text{C}_{14}\text{H}_{11}\text{ClO}_2\text{SSe}$  [ $\text{M} + \text{Na}$ ] $^+$  380.9226; found 380.9230.

**4.3.2.4. Methyl 2-(((4-bromophenyl)thio)selanyl)benzoate (11d).** Yellow solid; Yield 42 %; m.p. 101–102 °C;  $^1\text{H}$  NMR (400 MHz,  $\text{CDCl}_3$ )  $\delta$  8.12–8.06 (m, 2H, Ar-H), 7.51 (td,  $J = 8.2, 7.8, 1.5$  Hz, 1H, Ar-H), 7.39–7.28 (m, 5H, Ar-H), 3.99 (s, 3H,  $\text{OCH}_3$ );  $^{13}\text{C}$  NMR (101 MHz,  $\text{CDCl}_3$ )  $\delta$  168.1, 137.9, 135.5, 133.6, 131.9, 131.4, 130.4, 127.3, 127.2, 126.2, 120.5, 52.8;  $^{77}\text{Se}$  NMR (76 MHz,  $\text{CDCl}_3$ )  $\delta$  594.3; HRMS (ESI)  $m/z$  calcd for  $\text{C}_{14}\text{H}_{11}\text{BrO}_2\text{SSe}$  [ $\text{M} + \text{Na}$ ] $^+$  424.8721; found 424.8726.

**4.3.2.5. Methyl 2-(((4-nitrophenyl)thio)selanyl)benzoate (11e).** Pale-red solid; Yield 43 %; m.p. 131–132 °C;  $^1\text{H}$  NMR (400 MHz,  $\text{CDCl}_3$ )  $\delta$  8.13 (dd,  $J = 7.8, 1.3$  Hz, 1H, Ar-H), 8.10 (d,  $J = 9.0$  Hz, 2H, Ar-H), 7.95 (d,  $J = 8.1$  Hz, 1H, Ar-H), 7.62 (d,  $J = 8.9$  Hz, 2H, Ar-H), 7.55–7.49 (m, 1H, Ar-H), 7.36 (t,  $J = 7.1$  Hz, 1H, Ar-H), 4.04 (s, 3H,  $\text{OCH}_3$ );  $^{13}\text{C}$  NMR (101 MHz,  $\text{CDCl}_3$ )  $\delta$  168.4, 145.5, 137.1, 133.8, 131.6, 128.0, 127.0, 126.6, 126.4, 124.4, 124.0, 53.0;  $^{77}\text{Se}$  NMR (76 MHz,  $\text{CDCl}_3$ )  $\delta$  570.4; HRMS (ESI)  $m/z$  calcd for  $\text{C}_{14}\text{H}_{11}\text{NO}_4\text{SSe}$  [ $\text{M} + \text{Na}$ ] $^+$  391.9466; found 391.9470.

**4.3.2.6. Methyl 2-(((*o*-tolylthio)selanyl)benzoate (11f).** Yellow solid; Yield 56 %; m.p. 88–89 °C;  $^1\text{H}$  NMR (400 MHz,  $\text{CDCl}_3$ )  $\delta$  8.14 (d,  $J = 8.1$  Hz, 1H, Ar-H), 8.10 (dd,  $J = 7.8, 1.4$  Hz, 1H, Ar-H), 7.56–7.49 (m, 1H, Ar-H), 7.46 (dd,  $J = 7.4, 1.6$  Hz, 1H, Ar-H), 7.32 (t,  $J = 7.5$  Hz, 1H, Ar-H), 7.18 (d,  $J = 6.8$  Hz, 1H, Ar-H), 7.09 (pd,  $J = 7.2, 1.4$  Hz, 2H, Ar-H), 4.01 (s, 3H,  $\text{OCH}_3$ ), 2.57 (s, 3H,  $\text{CH}_3$ );  $^{13}\text{C}$  NMR (101 MHz,  $\text{CDCl}_3$ )  $\delta$  168.1, 138.4, 137.2, 134.9, 133.5, 131.4, 130.1, 129.1, 127.7, 127.3, 126.7, 126.0, 52.7, 20.7;  $^{77}\text{Se}$  NMR (76 MHz,  $\text{CDCl}_3$ )  $\delta$  567.1; HRMS (ESI)  $m/z$  calcd for  $\text{C}_{15}\text{H}_{14}\text{O}_2\text{SSe}$  [ $\text{M} + \text{Na}$ ] $^+$  360.9772; found 360.9775.

**4.3.2.7. Methyl 2-(((2-fluorophenyl)thio)selanyl)benzoate (11g).** Yellow solid; Yield 56 %; m.p. 78–79 °C.  $^1\text{H}$  NMR (400 MHz,  $\text{CDCl}_3$ )  $\delta$  8.20 (d,  $J = 8.1$  Hz, 1H, Ar-H), 8.05 (dd,  $J = 7.8, 1.3$  Hz, 1H, Ar-H), 7.55–7.49 (m, 1H, Ar-H), 7.47 (td,  $J = 7.7, 1.4$  Hz, 1H, Ar-H), 7.28 (t,  $J = 7.5$  Hz, 1H, Ar-H), 7.15 (q,  $J = 7.8, 6.9$  Hz, 1H, Ar-H), 7.00 (q,  $J = 8.1$  Hz, 2H, Ar-H), 3.96 (s, 3H,  $\text{OCH}_3$ );  $^{13}\text{C}$  NMR (101 MHz,  $\text{CDCl}_3$ )  $\delta$  168.2, 162.1, 159.6, 138.2, 133.6, 132.4, 131.3, 128.9, 128.8, 127.6, 127.1, 126.1, 124.8, 124.7, 115.6, 115.4, 52.8;  $^{77}\text{Se}$  NMR (76 MHz,  $\text{CDCl}_3$ )  $\delta$

594.1. HRMS (ESI)  $m/z$  calcd for  $\text{C}_{14}\text{H}_{11}\text{FO}_2\text{SSe}$  [ $\text{M} + \text{Na}$ ] $^+$  364.9521; found 364.9527.

**4.3.2.8. Methyl 2-(((2-chlorophenyl)thio)selanyl)benzoate (11h).** Yellow solid; Yield 41 %; m.p. 99–100 °C;  $^1\text{H}$  NMR (400 MHz,  $\text{DMSO}-d_6$ )  $\delta$  8.09 (d,  $J = 7.7$  Hz, 1H, Ar-H), 7.94 (d,  $J = 8.1$  Hz, 1H, Ar-H), 7.68 (t,  $J = 7.6$  Hz, 1H, Ar-H), 7.48 (dq,  $J = 15.0, 7.3$  Hz, 3H, Ar-H), 7.26 (p,  $J = 7.3$  Hz, 2H, Ar-H), 3.96 (s, 3H,  $\text{OCH}_3$ );  $^{13}\text{C}$  NMR (101 MHz,  $\text{DMSO}-d_6$ )  $\delta$  167.6, 136.1, 134.3, 133.5, 132.1, 131.4, 129.9, 129.7, 128.4, 128.3, 126.9, 126.7, 53.1;  $^{77}\text{Se}$  NMR (76 MHz,  $\text{DMSO}-d_6$ )  $\delta$  561.0. HRMS (ESI)  $m/z$  calcd for  $\text{C}_{14}\text{H}_{11}\text{ClO}_2\text{SSe}$  [ $\text{M} + \text{Na}$ ] $^+$  380.9226; found 380.9227.

**4.3.2.9. Methyl 2-(((2-bromophenyl)thio)selanyl)benzoate (11i).** Pale-yellow solid; Yield 52 %; m.p. 115–116 °C;  $^1\text{H}$  NMR (400 MHz,  $\text{CDCl}_3$ )  $\delta$  8.09 (d,  $J = 7.8$  Hz, 1H, Ar-H), 7.98 (d,  $J = 8.1$  Hz, 1H, Ar-H), 7.53 (d,  $J = 8.0$  Hz, 1H, Ar-H), 7.48 (d,  $J = 8.0$  Hz, 2H, Ar-H), 7.31 (t,  $J = 7.4$  Hz, 1H, Ar-H), 7.16 (t,  $J = 8.3$  Hz, 1H, Ar-H), 7.01 (t,  $J = 7.6$  Hz, 1H, Ar-H), 4.01 (d,  $J = 1.5$  Hz, 3H,  $\text{OCH}_3$ );  $^{13}\text{C}$  NMR (101 MHz,  $\text{CDCl}_3$ )  $\delta$  168.3, 137.6, 136.6, 133.7, 132.7, 131.4, 129.5, 128.1, 127.6, 127.5, 127.3, 126.2, 122.6, 52.9;  $^{77}\text{Se}$  NMR (76 MHz,  $\text{CDCl}_3$ )  $\delta$  561.8; HRMS (ESI)  $m/z$  calcd for  $\text{C}_{14}\text{H}_{11}\text{BrO}_2\text{SSe}$  [ $\text{M} + \text{Na}$ ] $^+$  424.8721; found 424.8722.

**4.3.2.10. Methyl 2-(((3-(trifluoromethyl)phenyl)thio)selanyl)benzoate (11j).** Yellow solid; Yield 27 %; m.p. 72–73 °C;  $^1\text{H}$  NMR (400 MHz,  $\text{CDCl}_3$ )  $\delta$  8.06 (td,  $J = 7.0, 6.3, 1.0$  Hz, 2H, Ar-H), 7.73 (s, 1H, Ar-H), 7.63 (d,  $J = 7.8$  Hz, 1H, Ar-H), 7.53–7.47 (m, 1H, Ar-H), 7.38 (d,  $J = 7.8$  Hz, 1H, Ar-H), 7.31 (q,  $J = 7.4, 6.9$  Hz, 2H, Ar-H), 3.98 (s, 3H,  $\text{OCH}_3$ );  $^{13}\text{C}$  NMR (101 MHz,  $\text{CDCl}_3$ )  $\delta$  168.2, 137.8, 137.7, 133.7, 131.9, 131.5, 131.1, 129.4, 127.2, 126.3, 125.3 (q,  $J = 3.8$  Hz), 125.1, 123.3 (q,  $J = 3.8$  Hz), 122.4, 52.6;  $^{77}\text{Se}$  NMR (76 MHz,  $\text{CDCl}_3$ )  $\delta$  586.1; HRMS (ESI)  $m/z$  calcd for  $\text{C}_{15}\text{H}_{11}\text{F}_3\text{O}_2\text{SSe}$  [ $\text{M} + \text{Na}$ ] $^+$  414.9489; found 414.9495.

**4.3.2.11. Methyl 2-(((3,5-bis(trifluoromethyl)phenyl)thio)selanyl)benzoate (11k).** Yellow solid; Yield 22 %; m.p. 75–76 °C;  $^1\text{H}$  NMR (400 MHz,  $\text{CDCl}_3$ )  $\delta$  8.14 (d,  $J = 7.8$  Hz, 1H, Ar-H), 8.01 (d,  $J = 8.1$  Hz, 1H, Ar-H), 7.93 (s, 2H, Ar-H), 7.66 (s, 1H, Ar-H), 7.56 (t,  $J = 8.4$  Hz, 1H, Ar-H), 7.37 (t,  $J = 7.5$  Hz, 1H, Ar-H), 4.05 (s, 3H,  $\text{OCH}_3$ );  $^{13}\text{C}$  NMR (101 MHz,  $\text{CDCl}_3$ )  $\delta$  168.4, 140.1, 137.0, 133.8, 132.2 (q,  $J = 33.4$  Hz), 131.6, 128.3, 128.2, 127.2, 126.8, 126.5, 124.3, 121.6, 120.3, 120.24, 120.20, 120.17, 120.13, 53.0;  $^{77}\text{Se}$  NMR (76 MHz,  $\text{CDCl}_3$ )  $\delta$  584.3; HRMS (ESI)  $m/z$  calcd for  $\text{C}_{16}\text{H}_{10}\text{F}_6\text{O}_2\text{SSe}$  [ $\text{M} + \text{Na}$ ] $^+$  482.9363; found 482.9366.

**4.3.2.12. Methyl 2-(((naphthalen-1-ylthio)selanyl)benzoate (11l).** Yellow solid; Yield 23 %; m.p. 68–69 °C;  $^1\text{H}$  NMR (400 MHz,  $\text{CDCl}_3$ )  $\delta$  8.21 (d,  $J = 7.6$  Hz, 1H, Ar-H), 8.08 (dd,  $J = 7.8, 1.4$  Hz, 1H, Ar-H), 7.96 (s, 1H, Ar-H), 7.77 (d,  $J = 7.6$  Hz, 1H, Ar-H), 7.71 (m, 2H, Ar-H), 7.59 (dd,  $J = 8.7, 1.9$  Hz, 1H, Ar-H), 7.54–7.47 (m, 1H, Ar-H), 7.43 (pd,  $J = 6.9, 1.4$  Hz, 2H, Ar-H), 7.33–7.26 (m, 1H, Ar-H), 4.00 (s, 3H,  $\text{OCH}_3$ );  $^{13}\text{C}$  NMR (101 MHz,  $\text{CDCl}_3$ )  $\delta$  168.2, 138.4, 133.6, 133.5, 133.5, 132.2, 131.4, 128.7, 127.7, 127.6, 127.3, 127.2, 126.9, 126.6, 126.0, 125.9, 52.7;  $^{77}\text{Se}$  NMR (76 MHz,  $\text{CDCl}_3$ )  $\delta$  586.5; HRMS (ESI)  $m/z$  calcd for  $\text{C}_{18}\text{H}_{14}\text{O}_2\text{SSe}$  [ $\text{M} + \text{Na}$ ] $^+$  396.9772; found 396.9775.

**4.3.2.13. Ethyl 2-(((*p*-tolylthio)selanyl)benzoate (11m).** Yellow solid; Yield 67 %; m.p. 54–55 °C;  $^1\text{H}$  NMR (400 MHz,  $\text{CDCl}_3$ )  $\delta$  8.07 (dd,  $J = 8.1, 0.8$  Hz, 1H, Ar-H), 7.93 (dd,  $J = 7.8, 1.4$  Hz, 1H, Ar-H), 7.36 (ddd,  $J = 8.6, 7.3, 1.5$  Hz, 1H, Ar-H), 7.25 (d,  $J = 8.2$  Hz, 2H, Ar-H), 7.14 (td,  $J = 7.8, 1.1$  Hz, 1H, Ar-H), 6.90 (d,  $J = 8.0$  Hz, 2H, Ar-H), 4.29 (q,  $J = 7.1$  Hz, 2H,  $\text{CH}_2$ ), 2.14 (s, 3H,  $\text{Ph}-\text{CH}_3$ ), 1.28 (t,  $J = 7.1$  Hz, 3H,  $\text{CH}_3$ );  $^{13}\text{C}$  NMR (101 MHz,  $\text{CDCl}_3$ )  $\delta$  167.6, 138.5, 136.8, 133.3, 132.9, 131.3, 129.7, 129.4, 127.5, 125.8, 61.8, 20.9, 14.5;  $^{77}\text{Se}$  NMR (76 MHz,  $\text{CDCl}_3$ )  $\delta$  602.3; HRMS (ESI)  $m/z$  calcd for  $\text{C}_{16}\text{H}_{16}\text{O}_2\text{SSe}$  [ $\text{M} + \text{Na}$ ] $^+$  374.9928; found 374.9932.

**4.3.2.14. Ethyl 2-(((4-chlorophenyl)thio)selanyl)benzoate (11n).** White

solid; Yield 19 %; m.p. 55–56 °C;  $^1\text{H}$  NMR (400 MHz,  $\text{CDCl}_3$ )  $\delta$  8.12 (dd,  $J = 5.3, 1.1$  Hz, 1H, Ar-H), 8.11–8.08 (m, 1H, Ar-H), 7.55–7.48 (m, 1H, Ar-H), 7.46–7.40 (m, 2H, Ar-H), 7.31 (t,  $J = 7.5$  Hz, 1H, Ar-H), 7.23–7.16 (m, 2H, Ar-H), 4.45 (q,  $J = 7.1$  Hz, 2H,  $\text{CH}_2$ ), 1.44 (t,  $J = 7.1$  Hz, 3H,  $\text{CH}_3$ );  $^{13}\text{C}$  NMR (101 MHz,  $\text{CDCl}_3$ )  $\delta$  167.7, 137.9, 134.9, 133.5, 132.6, 131.4, 130.2, 129.0, 127.4, 127.2, 126.1, 62.0, 14.3;  $^{77}\text{Se}$  NMR (76 MHz,  $\text{CDCl}_3$ )  $\delta$  597.3; HRMS (ESI)  $m/z$  calcd for  $\text{C}_{15}\text{H}_{13}\text{ClO}_2\text{SSe}$  [ $\text{M} + \text{Na}$ ] $^+$  394.9382; found 394.9382.

**4.3.2.15. Ethyl 2-(((4-bromophenyl)thio)selanyl)benzoate (11o).** Yellow solid; Yield 29 %; m.p. 57–58 °C;  $^1\text{H}$  NMR (400 MHz,  $\text{CDCl}_3$ )  $\delta$  8.09 (d,  $J = 9.2$  Hz, 2H, Ar-H), 7.50 (t,  $J = 8.4$  Hz, 1H, Ar-H), 7.38–7.32 (m, 4H, Ar-H), 7.30 (d,  $J = 7.0$  Hz, 1H, Ar-H), 4.45 (q,  $J = 7.1$  Hz, 2H,  $\text{CH}_2$ ), 1.44 (t,  $J = 7.1$  Hz, 3H,  $\text{CH}_3$ );  $^{13}\text{C}$  NMR (101 MHz,  $\text{CDCl}_3$ )  $\delta$  167.7, 137.8, 135.6, 133.5, 131.9, 131.4, 130.4, 127.5, 127.2, 126.1, 120.5, 61.9, 14.4;  $^{77}\text{Se}$  NMR (76 MHz,  $\text{CDCl}_3$ )  $\delta$  594.2; HRMS (ESI)  $m/z$  calcd for  $\text{C}_{15}\text{H}_{13}\text{BrO}_2\text{SSe}$  [ $\text{M} + \text{Na}$ ] $^+$  438.8877; found 438.8877.

**4.3.2.16. Ethyl 2-(((4-nitrophenyl)thio)selanyl)benzoate (11p).** White solid; Yield 26 %; m.p. 99–100 °C.  $^1\text{H}$  NMR (400 MHz,  $\text{CDCl}_3$ )  $\delta$  8.13 (d,  $J = 9.1$  Hz, 1H, Ar-H), 8.08 (d,  $J = 8.9$  Hz, 2H, Ar-H), 7.92 (d,  $J = 8.1$  Hz, 1H, Ar-H), 7.60 (d,  $J = 8.9$  Hz, 2H, Ar-H), 7.49 (t,  $J = 7.7$  Hz, 1H, Ar-H), 7.34 (t,  $J = 8.0$  Hz, 1H, Ar-H), 4.48 (q,  $J = 7.1$  Hz, 2H,  $\text{CH}_2$ ), 1.46 (t,  $J = 7.1$  Hz, 3H,  $\text{CH}_3$ );  $^{13}\text{C}$  NMR (101 MHz,  $\text{CDCl}_3$ )  $\delta$  168.0, 145.6, 137.0, 133.7, 131.5, 128.0, 127.6, 126.9, 126.5, 124.0, 62.2, 14.3;  $^{77}\text{Se}$  NMR (76 MHz,  $\text{CDCl}_3$ )  $\delta$  570.6; HRMS (ESI)  $m/z$  calcd for  $\text{C}_{15}\text{H}_{13}\text{NO}_4\text{SSe}$  [ $\text{M} + \text{Na}$ ] $^+$  405.9623; found 405.9623.

**4.3.2.17. Ethyl 2-(((2-fluorophenyl)thio)selanyl)benzoate (11q).** White solid; Yield 39 %; m.p. 86–87 °C;  $^1\text{H}$  NMR (400 MHz,  $\text{CDCl}_3$ )  $\delta$  8.21 (d,  $J = 7.9$  Hz, 1H, Ar-H), 8.08 (dd,  $J = 7.8, 1.5$  Hz, 1H, Ar-H), 7.56–7.45 (m, 2H, Ar-H), 7.33–7.27 (m, 1H, Ar-H), 7.16 (dtd,  $J = 9.4, 5.1, 1.7$  Hz, 1H, Ar-H), 7.05–6.97 (m, 2H, Ar-H), 4.43 (q,  $J = 7.1$  Hz, 2H,  $\text{CH}_2$ ), 1.42 (t,  $J = 7.1$  Hz, 3H,  $\text{CH}_3$ );  $^{13}\text{C}$  NMR (101 MHz,  $\text{CDCl}_3$ )  $\delta$  167.8, 162.1, 159.6, 138.1, 133.5, 132.4, 131.3, 128.8, 127.5, 126.0, 124.7, 123.7, 115.4, 62.0, 14.3;  $^{77}\text{Se}$  NMR (76 MHz,  $\text{CDCl}_3$ )  $\delta$  593.7; HRMS (ESI)  $m/z$  calcd for  $\text{C}_{15}\text{H}_{13}\text{FO}_2\text{SSe}$  [ $\text{M} + \text{Na}$ ] $^+$  378.9678; found 378.9680.

**4.3.2.18. Ethyl 2-(((2-chlorophenyl)thio)selanyl)benzoate (11r).** White solid; Yield 23 %; m.p. 62–63 °C;  $^1\text{H}$  NMR (400 MHz,  $\text{CDCl}_3$ )  $\delta$  8.10 (dd,  $J = 7.8, 1.4$  Hz, 1H, Ar-H), 8.04–7.98 (m, 1H, Ar-H), 7.48 (td,  $J = 7.1, 2.0$  Hz, 2H, Ar-H), 7.37–7.33 (m, 1H, Ar-H), 7.30 (td,  $J = 7.8, 1.1$  Hz, 1H, Ar-H), 7.14–7.06 (m, 2H, Ar-H), 4.46 (q,  $J = 7.1$  Hz, 2H,  $\text{CH}_2$ ), 1.45 (t,  $J = 7.1$  Hz, 3H,  $\text{CH}_3$ );  $^{13}\text{C}$  NMR (101 MHz,  $\text{CDCl}_3$ )  $\delta$  167.8, 137.6, 134.8, 133.6, 132.9, 131.4, 129.8, 129.5, 127.6, 127.5, 127.5, 127.4, 126.1, 62.0, 14.3;  $^{77}\text{Se}$  NMR (76 MHz,  $\text{CDCl}_3$ )  $\delta$  558.7; HRMS (ESI)  $m/z$  calcd for  $\text{C}_{15}\text{H}_{13}\text{ClO}_2\text{SSe}$  [ $\text{M} + \text{Na}$ ] $^+$  394.9382; found 394.9385.

**4.3.2.19. Ethyl 2-(((2-bromophenyl)thio)selanyl)benzoate (11s).** White solid; Yield 31 %; m.p. 74–75 °C;  $^1\text{H}$  NMR (400 MHz,  $\text{CDCl}_3$ )  $\delta$  8.10 (dd,  $J = 7.8, 1.4$  Hz, 1H, Ar-H), 8.00–7.96 (m, 1H, Ar-H), 7.53 (dd,  $J = 7.9, 1.2$  Hz, 1H, Ar-H), 7.51–7.45 (m, 2H, Ar-H), 7.31 (td,  $J = 7.8, 1.0$  Hz, 1H, Ar-H), 7.16 (td,  $J = 8.0, 1.3$  Hz, 1H, Ar-H), 7.01 (td,  $J = 7.7, 1.5$  Hz, 1H, Ar-H), 4.47 (q,  $J = 7.1$  Hz, 2H,  $\text{CH}_2$ ), 1.45 (t,  $J = 7.1$  Hz, 3H,  $\text{CH}_3$ );  $^{13}\text{C}$  NMR (101 MHz,  $\text{CDCl}_3$ )  $\delta$  167.8, 137.5, 136.7, 133.6, 132.7, 131.4, 129.5, 128.1, 127.6, 127.5, 127.5, 126.2, 122.7, 62.0, 14.4;  $^{77}\text{Se}$  NMR (76 MHz,  $\text{CDCl}_3$ )  $\delta$  562.0; HRMS (ESI)  $m/z$  calcd for  $\text{C}_{15}\text{H}_{13}\text{BrO}_2\text{SSe}$  [ $\text{M} + \text{Na}$ ] $^+$  438.8877; found 438.8875.

**4.3.2.20. Ethyl 2-(((3,5-bis(trifluoromethyl)phenyl)thio)selanyl)benzoate (11t).** Yellow solid; Yield 21 %; m.p. 93–94 °C;  $^1\text{H}$  NMR (400 MHz,  $\text{CDCl}_3$ )  $\delta$  8.13 (dd,  $J = 7.8, 1.4$  Hz, 1H, Ar-H), 7.99 (d,  $J = 7.7$  Hz, 1H, Ar-H), 7.92 (s, 2H, Ar-H), 7.64 (s, 1H, Ar-H), 7.57–7.49 (m, 1H, Ar-H), 7.38–7.32 (m, 1H, Ar-H), 4.48 (q,  $J = 7.1$  Hz, 2H,  $\text{CH}_2$ ), 1.46 (t,  $J = 7.1$  Hz, 3H,  $\text{CH}_3$ );  $^{13}\text{C}$  NMR (101 MHz,  $\text{CDCl}_3$ )  $\delta$  167.95, 140.15, 136.94, 133.71,

132.19 (q,  $J = 33.5$  Hz), 131.6, 128.3, 128.3, 127.6, 126.8, 126.5, 124.3, 121.6, 120.2 (p,  $J = 3.7$  Hz), 62.2, 14.3;  $^{77}\text{Se}$  NMR (76 MHz,  $\text{CDCl}_3$ )  $\delta$  584.6; HRMS (ESI)  $m/z$  calcd for  $\text{C}_{17}\text{H}_{12}\text{F}_6\text{O}_2\text{SSe}$  [ $\text{M} + \text{Na}$ ] $^+$  496.9520; found 496.9529.

**4.3.2.21. Ethyl 2-((naphthalen-2-ylthio)selanyl)benzoate (11u).** Yellow solid; Yield 22 %; m.p. 75–76 °C;  $^1\text{H}$  NMR (400 MHz,  $\text{CDCl}_3$ )  $\delta$  8.23 (d,  $J = 8.1$  Hz, 1H, Ar-H), 8.11 (dd,  $J = 7.8, 1.3$  Hz, 1H, Ar-H), 7.98 (s, 1H, Ar-H), 7.77 (d,  $J = 7.6$  Hz, 1H, Ar-H), 7.72 (dd,  $J = 8.0, 4.3$  Hz, 2H, Ar-H), 7.61 (dd,  $J = 8.7, 1.8$  Hz, 1H, Ar-H), 7.52–7.48 (m, 1H, Ar-H), 7.47–7.39 (m, 2H, Ar-H), 7.30 (t,  $J = 7.5$  Hz, 1H, Ar-H), 4.47 (q,  $J = 7.1$  Hz, 2H,  $\text{CH}_2$ ), 1.46 (t,  $J = 7.1$  Hz, 3H,  $\text{CH}_3$ );  $^{13}\text{C}$  NMR (101 MHz,  $\text{CDCl}_3$ )  $\delta$  167.7, 138.3, 133.6, 133.5, 133.5, 132.1, 131.5, 128.7, 127.6, 127.5, 127.3, 126.9, 126.6, 126.0, 125.9, 61.9, 14.4;  $^{77}\text{Se}$  NMR (76 MHz,  $\text{CDCl}_3$ )  $\delta$  586.6; HRMS (ESI)  $m/z$  calcd for  $\text{C}_{19}\text{H}_{16}\text{O}_2\text{SSe}$  [ $\text{M} + \text{Na}$ ] $^+$  410.9928; found 410.9935.

#### 4.4. Biological reagents and conditions

Sodium chloride, potassium chloride, disodium hydrogen phosphate dodecahydrate, potassium dihydrogen phosphate and dimethyl sulfide were purchased from National Pharmaceutical Group Chemical Reagent Co., Ltd. Tris-(hydroxymethyl)-aminomethane was purchased from Novon Scientific. Imidazole was purchased from MP Biomedicals. Dithiothreitol was purchased from Beijing Xinjingke Biotechnology Co., Ltd. Bovine serum albumin and glycerol were purchased from Sigma. Rupintrivir was purchased from Toronto Research Chemicals. Cell counting Kit-8 was purchased from Dojindo Chemicals. Substrate for the 3C<sup>pro</sup>/3C<sup>pro</sup> H-Asp-{Glu(EDANS)}-Met-Ser-Ala-Ile-Phe-Gln-Gly-Pro-Ile-Ser-{Lys(DABCYL)}-Asp-OH was purchased from GL Biochem in Shanghai. 96-well microtiter plates were purchased from Corning Co. Ltd. Enzyme inhibition and cell based activity was recorded on a Spectra max 190 microplate reader (Molecular Devices Co. Ltd.). All the experiments were conducted in a standard biosafety shelter laboratory 2 (BSL-2).

#### 4.5. Enzyme inhibition assay

EV71-3C<sup>pro</sup> and CVB3-3C<sup>pro</sup> were expressed and purified similar to the previous method (Lu et al., 2011; Wan et al., 2023). The DNA encoding EV71-3C or CVB3-3C protease was amplified and inserted into pET28a (Novagen). The resulting plasmid encodes an N-terminal His-tagged EV71-3C or CVB3-3C protease. For the expression and purification, the plasmid was transformed into Rosetta™ (DE3) Competent Cells (Novagen). Bacteria culture was grown in LB culture at 37 °C until the density OD<sub>600</sub> reached 1.0, after that IPTG was added to the culture (final concentration of 0.5 mM) to induce expression, which was shaken for another 20 h at 18 °C. Bacterial cells were collected by centrifugation at 4000 g, and resuspended in the lysis buffer that contained 50 mM Tris-HCl (pH 8.0), 150 mM NaCl and 20 mM imidazole. After that the bacterial cells were disrupted by ultra-sonication and cell debris was removed by centrifugation at 20,000 g for 1 h before the supernatant was loaded to Ni-nitrilotriacetic acid resin (GE Healthcare, USA) pre-equilibrated with the lysis buffer. Nonspecific contaminants were further removed by washing the resin with 10x bed volume of the wash buffer containing 50 mM Tris-HCl (pH 8.0), 150 mM NaCl, and 20 mM imidazole. For the next step the recombinant 3C proteins were eluted with the elution buffer containing 50 mM Tris-HCl (pH 8.0), 150 mM NaCl, and 300 mM imidazole. 6xHis-tag was cleaved by Thrombin (Sigma). In the end 3C protease was purified by gel-filtration (Superdex 200 column, GE Healthcare, USA) pre-equilibrated with the gel-filtration buffer that contained 25 mM HEPES (pH 8.0), 150 mM NaCl. Fractions containing 3C protease were pooled and concentrated to 5 mg/mL.

CVB3-3C<sup>pro</sup> inhibition assay was taken as an example here and the

assay for EV71-3C<sup>pro</sup> was highly similar. The tested compounds were dissolved in DMSO stock solutions of 50 mM concentration. The total volume of the reaction buffer was 50  $\mu$ L, which included 2.3  $\mu$ M of CVB3-3C<sup>pro</sup>, 25  $\mu$ M of substrate and PBS-BSA buffer (PBS buffer  $\times$  2 with 2 mg/mL BSA and 5.85 mg/mL NaCl), and 0–200  $\mu$ M of the tested compounds of double concentration gradient. Rupintrivir was selected as a control for comparison. The reaction was incubated at 37 °C for 60 min, followed by the fluorescence absorbance recorded by the microplate reader. The excitation/emission light was 340/490 nm. The IC<sub>50</sub> values were calculated by Eq. (1).

$$v = v_0 / (1 + [I] / IC_{50})(1)$$

where  $v$  is the inhibited rate,  $v_0$  is the uninhibited rate, and  $[I]$  indicates the concentration of the inhibitor. All the assays were finished in triplicate.

#### 4.6. Cell-based antiviral evaluations

The recombinant CVB3 and EV71 viruses were constructed using reverse genetic approaches from 12 plasmid system and restored in the Key Laboratory of Pathogenic Microorganisms and Immunology, Institute of Microbiology, Beijing. Good conditioned Hela cells were cultured in 12-well plates and incubated at 37 °C and 5 % CO<sub>2</sub> environmental condition for 24 h, and then the culture medium was changed to DMEM medium for 1 h. After that the inhibitors were added to the medium in different concentrations and incubated for 40 min. Subsequently, the Hela cells were infected by CVB3 or EV71 with a multiplicity of infection (MOI) of 0.1. The positive control only contained the Hela cells and did not contain the inhibitor and the virus, and the negative control contained the Hela cells and the virus. A further 16 h incubation was performed until the negative control exhibited obvious cytopathic effect (CPE) and then the cell viability was measured using the MTS reagent. The IC<sub>50</sub> values were calculated by equation (2).

$$IC_{50} = [C_L(I_H - 50) + C_H(50 - I_L)] / (I_H - I_L)(2)$$

where  $C_L$  means low concentration and  $I_L$  means inhibitory data at this concentration, while  $C_H$  means high concentration and  $I_H$  means inhibitory data at this condition. All the assays were evaluated in triplicate.

Viral titer was determined by the viral plaque assay. In detail, when Hela cells reached 95 % density, the cells were infected by different concentrations of CVB3 for 1 h. After washed by PBS, DMEM containing 1.5 % low melting point agarose and 2 mg/L pancreatic enzyme was added. After 3 d incubation, the viral plaque was counted.

The cytotoxicity assay was similar to the above cell-based antiviral experiment, and the only difference was that the Hela cells were not infected by the virus.

#### 4.7. Molecular docking

The molecular structure of the **11f** was constructed within Sybyl 7.3 (Tripos Inc., St Louis, MO), based on the crystal structure of **11 s**. The structure model was assigned Gasteiger-Hückel charges and minimized by the Tripos force field. FlexX module was used to carry out the molecular docking task. The crystal structure of EV71-3C<sup>pro</sup> in complex with rupintrivir (pdb code 3sjo) was retrieved from the pdb databank. All water molecules were removed, and hydrogen atoms were added in the standard geometry. Any amino acid residue within 5.0 Å of the location of rupintrivir was considered to be in the binding pocket. Cscore calculation was enabled and set to serial mode. The scoring procedures were performed using the default parameters in the program.

#### 4.8. Comparative field analysis

All the 3D structures of the compounds were built based on the

structure of **11f** from molecular docking result and treated using same manner within Sybyl 7.3. All the parameters were used the default value within CoMFA module and the column filtering was set to 2.0 kcal/mol. The “leave-one-out” (LOO) cross validation method was tried to determine the optimum number of partial least squares (PLS) components. Finally, the non-cross validated method was used to derive the model to explain the quantitative structure-activity relationship.

#### CRediT authorship contribution statement

**Jin-Yin Tang:** Methodology, Investigation. **Shengwang Dai:** Methodology, Investigation. **Xiaofang Wang:** Visualization, Investigation. **Mengting Zhang:** Data curation, Resources. **Jin-Rui Shi:** Validation, Formal analysis. **Yong-Xuan Hong:** Formal analysis. **Zhi-Juan Sun:** Data curation. **Huan-Qin Dai:** Funding acquisition, Writing – review & editing, Project administration, Software, Supervision. **Jian-Guo Wang:** Conceptualization, Funding acquisition, Writing – original draft, Writing – review & editing, Project administration, Software, Supervision.

#### Declaration of competing interest

The authors declare that they have no known competing financial interests or personal relationships that could have appeared to influence the work reported in this paper.

#### Acknowledgment

This research was financially supported by the National Key Research and Development Program of China (No. 2017YFE0108200), National Natural Science Foundation of China (No. 22277060 and No. 22277135), and Department of New Drug Registration, Hebei Immune Cell Application Engineering Research Center/Baoding Newish Technology Co., Ltd.

#### Appendix A. Supplementary material

Supplementary data to this article can be found online at <https://doi.org/10.1016/j.arabjc.2024.105713>.

#### References

- Alberto, E.E., Braga, A.L., Detty, M.R., 2012. Imidazolium-containing diselenides for catalytic oxidations with hydrogen peroxide and sodium bromide in aqueous solutions. *Tetrahedron* 68 (51), 10476–10481. <https://doi.org/10.1016/j.tet.2012.08.004>.
- Ampornadanai, K., Meng, X., Shang, W., Jin, Z., Rogers, M., Zhao, Y., Rao, Z., Liu, Z.J., Yang, H., Zhang, L., O'Neill, P.M., Samar, H., S., 2021. Inhibition mechanism of SARS-CoV-2 main protease by ebsele and its derivatives. *Nat. Commun.* 12 (1), 3061. <https://doi.org/10.1038/s41467-021-23313-7>.
- Bhabak, K.P., Muges, G., 2007. Synthesis, characterization, and antioxidant activity of some ebsele analogues. *Chem. A Eur. J.* 13 (16), 4594–4601 <https://doi.org/10.1002/anie.200700004>.
- Bondock, S., Albarqi, T., Nasr, T., Mohamed, N.M., Abdou, M.M., 2023. Design, synthesis, cytotoxic evaluation and molecular docking of novel 1, 3, 4-thiadiazole sulfonamides with azene and coumarin moieties as carbonic anhydrase inhibitors. *Arab. J. Chem.* 16 (8), 104956. <https://doi.org/10.1016/j.arabjc.2023.104956>.
- Cannalire, R., Cerchia, C., Beccari, A.R., Di Leva, F.S., Summa, V., 2022. Targeting SARS-CoV-2 proteases and Polymerase for COVID-19 treatment: state of the art and future opportunities. *J. Med. Chem.* 65 (4), 2716–2746. <https://doi.org/10.1021/acs.jmedchem.0c01140>.
- Chen, R., Gao, Y., Liu, H., Li, H., Chen, W., Ma, J., 2023. Advances in research on 3C-like protease (3CLpro) inhibitors against SARS-CoV-2 since 2020. *RSC Medicinal Chemistry* 14 (1), 9–21. <https://doi.org/10.1039/d2md00344a>.
- Cheng, Y., Wu, J., Han, Y., Xu, J., Da, Y., Zhao, Q., Guo, G., Zhou, Y., Chen, Y., Liu, J., Chen, H., Jiang, X., Cai, X., 2021. A CDR-based approach to generate covalent inhibitory antibody for human rhinovirus protease. *Bioorg. Med. Chem.* 42, 116219 <https://doi.org/10.1016/j.bmc.2021.116219>.
- Chipoline, I.C., Brasil, B.F.A.B., Neto, J.S.S., Valli, M., Krogh, R., Cenci, A.R., Teixeira, K. F., Zapp, E., Brondani, D., Ferreira, L.L.G., Andricopulo, A.D., de Oliveira, A.S., Nascimento, V., 2022. Synthesis and investigation of the trypanocidal potential of novel 1,2,3-triazole-selenide hybrids. *Eur. J. Med. Chem.* 243, 114687 <https://doi.org/10.1016/j.ejmech.2022.114687>.

- Cramer, R.D., Patterson, D.E., Bunce, J.D., 1988. Comparative molecular field analysis (CoMFA). 1. effect of shape on binding of steroids to carrier proteins. *J. Am. Chem. Soc.* 110 (18), 5959–5967. <https://doi.org/10.1021/ja00226a005>.
- Dakova, B., Lamberts, L., Evers, M., Dereu, N., 1991. Electrochemical behavior of pharmacologically interesting seleno-organic compounds - 2. 7-substituted-N-aryl-1,2-benzisoxazol-3(2H)-one. *Electrochim. Acta* 36 (3–4), 631–637. [https://doi.org/10.1016/0013-4686\(91\)85151-V](https://doi.org/10.1016/0013-4686(91)85151-V).
- Diesendruck, C.E., Tzur, E., Ben-Asuly, A., Goldberg, I., Straub, B.F., Lemcoff, N.G., 2009. Predicting the cis-trans dichloro configuration of group 15–16 chelated ruthenium olefin metathesis complexes: a DFT and experimental study. *Inorg. Chem.* 48 (22), 10819–10825. <https://doi.org/10.1021/ic901444c>.
- Han, S.H., Goins, C.M., Arya, T., Shin, W.J., Maw, J., Hooper, A., Sonawane, D.P., Porter, M.R., Bannister, B.E., Crouch, R.D., Lindsey, A.A., Lakatos, G., Martinez, S.R., Alvarado, J., Akers, W.S., Wang, N.S., Jung, J.U., Macdonald, J.D., Stauffer, S.R., 2022. Structure-based optimization of ML300-derived, noncovalent inhibitors Targeting the severe acute respiratory syndrome coronavirus 3CL protease (SARS-CoV-2 3CLpro). *J. Med. Chem.* 65 (4), 2880–2904. <https://doi.org/10.1021/acs.jmedchem.1c00598>.
- Jin, Z., Du, X., Xu, Y., Deng, Y., Liu, M., Zhao, Y., Zhang, B., Li, X., Zhang, L., Peng, C., Duan, Y., Yu, J., Wang, L., Yang, K., Liu, F., Jiang, R., Yang, X., You, T., Liu, X., Yang, X., Bai, F., Liu, H., Liu, X., Guddat, L.W., Xu, W., Xiao, G., Qin, C., Shi, Z., Jiang, H., Rao, Z., Yang, H., 2020. Structure of m<sup>pro</sup> from SARS-CoV-2 and discovery of its inhibitors. *Nature* 582 (7811), 289–293. <https://doi.org/10.1038/s41586-020-2223-y>.
- Jones, P.G., Wismach, C., Mugesch, G., du Mont, W.W., 2002. Methyl 2-selenocyanatobenzoate. *Acta Crystallogr. Sect. E: Struct. Rep. Online* 58 (11), o1298–o1300. <https://doi.org/10.1107/S1600536802019323>.
- Krilov, L.R., 2004. Emerging infectious disease issues in international adoptions: severe acute respiratory syndrome (SARS), avian influenza and measles. *Curr. Opin. Infect. Dis.* 17 (5), 391–395. <https://doi.org/10.1097/00001432-200410000-00002>.
- Li, J., Lai, S., Gao, G.F., Shi, W., 2021. The emergence, genomic diversity and global spread of SARS-CoV-2. *Nature* 600 (7889), 408–418. <https://doi.org/10.1038/s41586-021-04188-6>.
- Lu, G., Qi, J., Chen, Z., Xu, X., Gao, F., Lin, D., Qian, W., Liu, H., Jiang, H., Yan, J., Gao, G.F., 2011. Enterovirus 71 and coxsackievirus A16 3C proteases: binding to rupintrivir and their substrates and anti-hand, foot, and mouth disease virus drug design. *J. Virol.* 85 (19), 10319–10331. <https://doi.org/10.1128/JVI.00787-11>.
- Lun, M.M., Su, C.Y., Li, J., Jia, Q.Q., Lu, H.F., Fu, D.W., Zhang, Y., Zhang, Z.X., 2023. Introducing ferroelasticity into 1D hybrid Lead Halide Semiconductor by halogen substitution strategy. *Small* 19, 2303127. <https://doi.org/10.1002/sml.202303127>.
- Luz, A.B.S., de Medeiros, A.F., Bezerra, L.L., Lima, M.S.R., Pereira, A.S., E. Silva, E.G.O., Passos, T.S., Monteiro, N.K.V., Morais, A.H.A., 2023. Prospecting native and analogous peptides with anti-SARS-CoV-2 potential derived from the trypsin inhibitor purified from tamarind seeds. *Arab. J. Chem.* 16 (8), 104886. <https://doi.org/10.1016/j.arabj.2023.104886>.
- Ma, C., Hu, Y., Townsend, J.A., Lagarias, P.I., Marty, M.T., Kolocouris, A., Wang, J., 2020. Ebselen, disulfiram, Carmofur, PX-12, tideglusib, and shikonin are nonspecific promiscuous SARS-CoV-2 Main protease inhibitors. *ACS Pharmacology & Translational Science* 3 (6), 1265–1277. <https://doi.org/10.1021/acscptsci.0c00130>.
- Mašlanka, M., Mucha, A., 2023. Antibacterial activity of ebselen. *Int. J. Mol. Sci.* 24 (2), 1610. <https://doi.org/10.3390/ijms24021610>.
- Meng, F.F., Sun, X.W., Shang, M.H., Zhang, J.S., Niu, C.W., Li, Y.H., Wang, Z.W., Wang, J.G., Li, Z.M., 2022. Chemical preparation, degradation analysis, computational docking and biological activities of novel sulfonylureas with 2,5-disubstituted groups. *Pestic. Biochem. Physiol.* 188, 105261. <https://doi.org/10.1016/j.pestbp.2022.105261>.
- Mohammad, T., Shamsi, A., Anwar, S., Umair, M., Hussain, A., Rehman, M.T., AlAjmi, M. F., Islam, A., Hassan, M.I., 2020. Identification of high-affinity inhibitors of SARS-CoV-2 main protease: Towards the development of effective COVID-19 therapy. *Virus Res.* 288, 198102. <https://doi.org/10.1016/j.virusres.2020.198102>.
- Nayak, G., Bhuyan, S.K., Bhuyan, R., Sahu, A., Kar, D., Kuanar, A., 2022. Global emergence of enterovirus 71: a systematic review. *BeniSuef University Journal of Basic and Applied Sciences* 11 (1), 78. <https://doi.org/10.1186/s43088-022-00258-4>.
- Noguchi, N., 2016. Ebselen, a useful tool for understanding cellular redox biology and a promising drug candidate for use in human diseases. *Arch. Biochem. Biophys.* 595, 109–112. <https://doi.org/10.1016/j.abb.2015.10.024>.
- Parnham, M., Sies, H., 2000. Ebselen: prospective therapy for cerebral ischaemia. *Expert Opin. Invest. Drugs* 9 (3), 607–619. <https://doi.org/10.1517/13543784.9.3.607>.
- Ramajayam, R., Tan, K.P., Liang, P.H., 2011. Recent development of 3C and 3CL protease inhibitors for anti-coronavirus and anti-picornavirus drug discovery. *Biochem. Soc. Trans.* 39 (5), 1371–1375. <https://doi.org/10.1042/BST0391371>.
- Salerno, M., Varricchio, C., Bevilacqua, F., Jochmans, D., Neyts, J., Brancale, A., Ferla, S., Bassetto, M., 2023. Rational design of novel nucleoside analogues reveals potent antiviral agents for EV71. *Eur. J. Med. Chem.* 246, 114942. <https://doi.org/10.1016/j.ejmech.2022.114942>.
- Sanmartin, C., Plano, D., Font, M., Palop, J.A., 2011. Selenium and clinical trials: new therapeutic evidence for multiple diseases. *Curr. Med. Chem.* 18 (30), 4635–4650. <https://doi.org/10.2174/092986711797379249>.
- Shang, M.H., Sun, X.W., Wang, H.L., Li, H.R., Zhang, J.S., Wang, L.Z., Yu, S.J., Zhang, X., Xiong, L.X., Li, Y.H., Niu, C.W., Wang, J.G., 2023. Facile synthesis, crystal structure, quantum calculation, and biological evaluations of novel selenenyl sulfide compounds as potential agrochemicals. *Pest Manag. Sci.* 79 (5), 1885–1896. <https://doi.org/10.1002/ps.7382>.
- Singh, B.G., Kunwar, A., 2021. Redox reactions of organoselenium compounds: implication in their biological activity. *Free Radic. Res.* 55 (6), 641–654. <https://doi.org/10.1080/10715762.2021.1882678>.
- Stubbing, L.A., Hubert, J.G., Bell-Tyrer, J., Hermant, Y.O., Yang, S.H., McSweeney, A.M., McKenzie-Goldsmith, G.M., Ward, V.K., Furkert, D.P., Brimble, M.A., 2023. P1 glutamine isosteres in the design of inhibitors of 3C/3CL protease of human viruses of the Pisoniviricetes class. *RSC Chemical Biology* 4 (8), 533–547. <https://doi.org/10.1039/d3cb00075c>.
- Tan, B., Joyce, R., Tan, H., Hu, Y., Wang, J., 2023. SARS-CoV-2 Main protease drug design, assay development, and drug resistance studies. *Acc. Chem. Res.* 56 (2), 157–168. <https://doi.org/10.1021/acs.accounts.2c00735>.
- Wan, L., Wang, X., Wang, T., Yuan, X., Liu, W., Huang, Y., Deng, C., Cao, S., 2023. Comparison of Target pocket Similarity and Progress into Research on inhibitors of picornavirus 3C proteases. *Chem. Biodivers.* 20 (3), e202201100.
- Wang, L., Bao, B.B., Song, G.Q., Chen, C., Zhang, X.M., Lu, W., Wang, Z., Cai, Y., Li, S., Fu, S., Song, F.H., Yang, H., Wang, J.G., 2017. Discovery of unsymmetrical aromatic disulfides as novel inhibitors of SARS-CoV main protease: chemical synthesis, biological evaluation, molecular docking and 3D-QSAR study. *Eur. J. Med. Chem.* 137, 450–461. <https://doi.org/10.1016/j.ejmech.2017.05.045>.
- Wang, J., Hu, Y., Zheng, M., 2022. Enterovirus A71 antivirals: past, present, and future. *Acta Pharm. Sin. B* 12 (4), 1542–1556. <https://doi.org/10.1016/j.apsb.2021.08.017>.
- Yoosefian, M., Dashti, R., Mahani, M., Montazer, L., Mir, A., 2023. A suitable drug structure for interaction with SARS-CoV-2 main protease between bocoprevir, masitinib and rupintrivir; a molecular dynamics study. *Arab. J. Chem.* 16 (9), 105051. <https://doi.org/10.1016/j.arabj.2023.105051>.
- Zang, Y., Su, M., Wang, Q., Cheng, X., Zhang, W., Zhao, Y., Chen, T., Jiang, Y., Shen, Q., Du, J., Tan, Q., Wang, P., Gao, L., Jin, Z., Zhang, M., Li, C., Zhu, Y., Feng, B., Tang, B., Xie, H., Wang, M.W., Zheng, M., Pan, X., Yang, H., Xu, Y., Wu, B., Zhang, L., Rao, Z., Yang, X., Jiang, H., Xiao, G., Zhao, Q., Li, J., 2022. High-throughput screening of SARS-CoV-2 main and papain-like protease inhibitors. *Protein Cell* 14 (1), 17–27. <https://doi.org/10.1093/procel/pwac016>.
- Zeng, Q.X., Wang, H.Q., Wei, W., Guo, T.T., Yu, L., Wang, Y.X., Li, Y.H., Song, D.Q., 2020. Synthesis and biological evaluation of berberine derivatives as a new class of broad-spectrum antiviral agents against coxsackievirus B. *Bioorg. Chem.* 95, 103490. <https://doi.org/10.1016/j.bioorg.2019.103490>.
- Zhang, L.X., Wang, J.G., Dai, H.Q., Zhang, X.M., Wang, Q.Q., Song, F.H., Shang, J., Wang, L.Q., Ma, R., 2016. Application of asymmetric aromatic disulfide compound as virus 3C protease inhibitor in preparing antiviral agent, CN 105640951 A.
- Zhang, L., Lin, D., Sun, X., Curth, U., Drosten, C., Sauerhering, L., Becker, S., Rox, K., Hilgenfeld, R., 2020. Crystal structure of SARS-CoV-2 main protease provides a basis for design of improved  $\alpha$ -ketoamide inhibitors. *Science* 368 (6489), 409–412. <https://doi.org/10.1126/science.abb3405>.
- Zhao, L.M., Pannecoque, C., Clercq, E.D., Wang, S., Chen, F.E., 2023. Structure-directed expansion of biphenyl-pyridone derivatives as potent non-nucleoside reverse transcriptase inhibitors with significantly improved potency and safety. *Chin. Chem. Lett.* 34 (12), 108261. <https://doi.org/10.1016/j.ccl.2023.108261>.
- Zhou, J., Chen, R., 1999. Synthesis and crystal structure of 2-phosphonoalkyl-1,2-benzisoxazol-3(2H)-ones and their antitumor activities. *Heteroat. Chem.* 10 (3), 247–254. [https://doi.org/10.1002/\(SICI\)1098-1071\(1999\)10:3<247::AID-HC12>3.0.CO;2-](https://doi.org/10.1002/(SICI)1098-1071(1999)10:3<247::AID-HC12>3.0.CO;2-).
- Zhu, G., Wu, C., Wang, Q., Deng, D., Lin, B., Hu, X., Qiu, F., Li, Z., Huang, C., Yang, Q., Zhang, D., 2023. Antiviral activity of the HSP90 inhibitor VER-50589 against enterovirus 71. *Antiviral Res.* 211, 105553. <https://doi.org/10.1016/j.antiviral.2023.105553>.